How Muscle Stiffness affects Neural Control Parameters

Short-Range Stiffness Improves Stability and Feedback Robustness of Musculoskeletal Models

Axel Milan Gründemann

How Muscle Stiffness affects Neural Control Parameters

Short-Range Stiffness Improves Stability and Feedback Robustness of Musculoskeletal Models

21/03/23

4603273

In partial fulfilment of the requirements for the degree of
Master of Science

In Biomedical Engineering

At the Delft University of Technology

By

Axel M. GRÜNDEMANN

[1] **Thesis Supervisors**

Ir. Elias Mateo Fernandez Santoro	Erasmus Medical Center
Dr. Ir. Mario Negrello	Erasmus Medical Center
Dr. Ir. Winfred Mugge	Delft University of Technology
Prof. Ir. Frans van der Helm	Delft University of Technology
Daily Supervisor:	
Ir. Elias Mateo Fernandez Santoro	Erasmus Medical Center

[1] Frontpage image from https://www.pngwing.com/es/free-png-sddkl

PREFACE

I'd like to thank my wonderful family and friends for supporting me through the many months of plotting and simulating muscles. I'd also like to thank all my supervisors, especially Frans for getting my project back on track and Mario for the many insightful conversations. Now that the project is finished, I can say with humour that I had been running my simulations hundreds of times too slowly because of a simple mistake.. which I found out a week before the draft deadline. I guess the real lesson is one of early perfectionism.

Axel M. Gründemann
Delft, April 2023

How Muscle Stiffness affects Neural Control Parameters

A. M. Gründemann
26/02/2023

This paper investigates the effect of intrinsic muscle stiffness on neural control parameters in biological musculoskeletal control of stabilisation or reaching tasks. Current model implementations of intrinsic muscle properties are highly simplified, limiting their accuracy in replicating experimental short-range stiffness (SRS) behaviour[1][2], which appears to be important for stabilisation tasks[3][4][5]. The Hill model[6], often used in musculoskeletal simulations[7], cannot account for SRS, while the Huxley model[8], which can account for non-linear muscle phenomena such as SRS[2], has a higher computational burden[7][9][10]. The study compares a simplified Huxley-type model[8][11] to two Hill-type models[6][2][12] and determines the effect of intrinsic SRS on the control parameters of stabilizing 1- and 2-Degree of Freedom musculoskeletal models over various positive and negative stiffness positions in the force-length curve. Furthermore, the effect of the intrinsic muscle stiffness on the robustness of the feedback parameters of simple individual muscle feedback systems is determined in reaching experiments similar to classic experiments in Flash and Hogan [13].

The study finds that the Huxley model shows positive SRS in the negative flank of the force-length curve, achieves stabilisation through only co-contraction using a lower level of required muscle excitation than both Hill-type models and stabilises both musculoskeletal systems at a larger muscle range than the Hill-type models, including in the negative stiffness flank. The feedback parameters dominantly responsible for muscle activation patterns are also more robust to change in the Huxley model. These findings suggest that intrinsic muscle stiffness impacts neural control parameters in stabilisation and reaching tasks, and further musculoskeletal modelling should consider using more complex muscle stiffness calculations for improved accuracy.

1 Introduction

Knowledge of the neural control of human movement is interesting for understanding movement disorders and for robotic applications and much is still unknown. The dominant framework in sensorimotor control[14] is optimal feedback control theory (OFC) and while it allows for many successful predictions of experimental motor behaviour[14][15], there is some evidence that casts doubt on its biological realism[16][17]. Consequently, improving the modelling accuracy of some of the mechanical intricacies of the neural controller could shed light on the differences between theory and biology. Information on a controller, such as the magnitude of applied gain, can logically be obtained by having systems with different properties controlled by it. It is therefore interesting to see what types of nonlinear behaviours arise in the musculoskeletal system, so we can test how the neural controller is able to deal with them.

An example of the control scheme for musculoskeletal stabilisation is given in Fig. 1.1. Here we can see how the success of a stabilisation or position task is dependent on both the intrinsic and the reflex feedback pathway. While active stabilisation is achieved by the generation of muscle activation patterns through the reflex pathway, the passive part of stabilisation is a consequence of the muscle behaviour itself through the intrinsic pathway.

Muscle behaviour is non-linear, and its response is a result of the visco-elasticity of the anatomical structures as well as dynamic changes of muscle stiffness. The way muscle stiffness is modelled depends on what muscle model is used. The goal of this thesis is to test how intrinsic muscle model stiffness complexity affects the magnitude of control parameters responsible for feed-forward stabilisation and robustness of the feedback parameters influencing reaching movements in a musculoskeletal testbed.

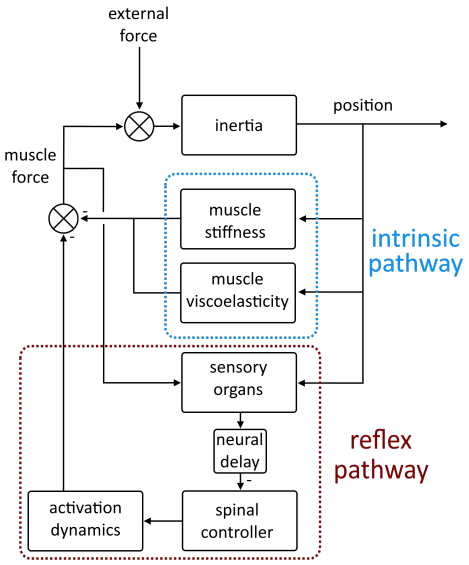

Figure 1.1.: A simplified control scheme for stabilisation tasks, highlighting both the intrinsic and the reflex feedback pathways. The reflex pathway consists of information from the proprioceptive organs being fed through the spinal cord and motor neurons, leading to muscle excitation. The intrinsic pathway is a faster force response as a result of the intrinsic properties of the muscle itself. Adapted from de Vlugt *et al.* [18] and de Vlugt [19].

The standard force-length (FL) curve of a muscle is depicted in Fig. 1.2.b. According to classical biomechanical theory[20], a muscle that is stretched beyond its optimal length

will respond with a reduction in produced force. This occurs in the negative stiffness flank of the FL curve, as depicted in Fig. 1.2.b. Experimental evidence suggests that a small local stretch in the negative stiffness flank could instead lead to an increase in force production, due to the muscle phenomenon known as short-range stiffness (SRS)[1]. The positive stiffness SRS can provide stability to the muscle-tendon complex (MTC) in an area that would theoretically be considered unstable[21], which is what makes it an interesting research area[22] within the intrinsic feedback path.

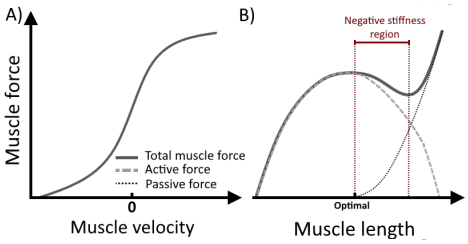

Figure 1.2.: (A) The force-velocity (FV) curve of a standard muscle. Simplified and adapted from Winters [10]. (B) The force-length (FL) curve of a standard muscle. Simplified and adapted from Knudson [23]. At a muscle length of smaller than the optimal length, the contribution of the passive force to the total muscle force is negligible. At a muscle length larger than the optimal length, the passive force starts to increase while the active force decreases. The negative stiffness flank of the FL curve starts at the optimal length and ends at the length where the passive force overtakes the active force.

There are two mainly used descriptive models of muscle contraction dynamics, the Hill-type[6][24] and the Huxley-type[8]. Hill-type models are considered relatively simple and effective at describing muscle behaviour in most applications[7]. The main downside of the Hill-type models is that, due to their simplicity, they fail to describe certain specific non-linear experimental behaviours, such as SRS [2], which is important for balancing tasks[3][4]. Shue, Crago and Chizeck [25] state that the Hill-type models fail to capture the effects of changing force levels and modulation depths that appear in experimental data.

The Huxley-type model is more detailed than the Hill-type model [7][9] and can account for many more non-linear muscle phenomena[10] because the Huxley-type includes the cross-bridge attachment dynamics in its calculations while linking the muscle stiffness to the cross-bridge stiffness. Cross-bridges are the molecular bonds formed between actin and myosion strands within a muscle and are responsible for muscle force generation. According the Huxley [8] model, the cross-bridges cycle between an attached force-generating state and a detached non-force generating state. Muscle force increases with the number of cross-bridges that are in active turnover between the two states. The Huxley model derives its force production from a modelled cross-bridge distribution, where cycling of the individual cross-bridges is calculated using with attachment and detachment rate functions. The curvature of the classic Hill-type model force-velocity (FV) relationship is depicted in Fig. 1.2.a. Most musculoskeletal models, like the Hill model, simplify the intrinsic feedback pathway by including the FL and the FV curves explicitly as parameterised functions, calculating the muscle force as some combination of the two. In contrast to the Hill model, the muscle stiffness and damping are emergent properties of the original Huxley equations, depending on how its rate functions are defined[26][27]. As a consequence, FV behaviour is a function of the cross-bridge attachment functions and does not need to be included explicitly like in the Hill-type models. The downside of the Huxley model is generally considered to be its high computational burden[7][9][10].

Since the goal is to analyse the effect of different ways intrinsic muscle stiffness can be calculated on the control parameters of the system, the first step must be to investigate the scope of these differences. This leads us to the problem statement, as well as the first hypothesis and sub-hypothesis:

Problem statement: *Current musculoskeletal models lack sufficiently detailed intrinsic muscle stiffness calculations, which affects the accuracy of neural control applications.*

Hypothesis 1: *A Huxley-type muscle model will intrinsically display positive stiffness behaviour under local stretch in the negative stiffness flank of the force-length curve, whereas a non-augmented Hill-type model will not.*
Sub-hypothesis 1.a: *The response to local stretch in the Huxley model will be a result of intrinsic cross-bridge stiffness rather than a result of the force-velocity relationship.*

The next step is to investigate the effect of the SRS on the control parameters of the neural controller. This can be accomplished by testing its effect on a known control strategy. Stabilisation of parts of the human body can be produced as a combination of active, passive and neural control subsystems[28], depending on the experiment task and locality. The neural control subsystem can in essence choose to enact certain strategies that can help stabilise the system. One of the strategies that the neural controller can employ for stabilisation is the co-contraction of antagonist muscles[29]. As co-contraction is essentially a method of achieving stability by increasing muscle damping, its efficacy relies on the dynamics of the intrinsic muscle properties. Results by De Groote, Allen and Ting [3] show that a Hill-type model augmented with an explicit SRS model provided improved stability against external perturbations in co-contraction experiments. Specifically, it showed improved stability during the neural delay period associated with the reflex pathway, meaning this behaviour must find its origin in the intrinsic feedback path. It then follows that a muscle model that produces SRS behaviour also implicitly improves the biological accuracy of the intrinsic feedback path, which in turn should improve stability. This brings us to the next hypothesis:

Hypothesis 2: *A muscle system that is stabilised through forward dynamic co-contraction will require a lower degree of muscle excitation when actuated by a Huxley-type muscle model when compared to a Hill-type muscle model.*

Results by Shabani and Stavness [5] show that realistic short-range stiffness has a larger impact on postural stability than co-contraction alone, which is more evidence for the hypothesis. We do not exactly know what hierarchical level of neural control is required for the execution of simple

learned reaching movements[30][31] or what a control variable in such a neural command would even look like[32][33]. Consequently, we do not know whether one muscle in a group that performs a reaching movement obtains proprioceptive information from the others during the movement or not[30]. As a result, our models assume reflex-like endpoint control without proprioceptive feedback. Controlling a musculoskeletal system through individual muscle feedback patterns is expected to be more difficult when using a standard Hill-type muscle model compared to a more complex Huxley-type muscle model that exhibits certain self-stabilising behaviours[3]. Evidence for this is found in the robustness of feedback parameters. If reaching movements made by the Huxley model are more robust to the changing of feedback parameters, then that must mean control parameters in the neural controller are more dependent on the intrinsic stiffness of the muscle itself than previously thought. Finally, we arrive at the last hypothesis:

Hypothesis 3: *The feedback parameters of individual muscles optimised for an end-point error task on a 2DoF musculoskeletal model should be more robust when actuated by a Huxley-type muscle model when compared to a Hill-type muscle model.*

1.1. APPROACH

To answer the three hypotheses, three experiments have been designed.

- The first experiment will simulate the muscles responding to forced stretching and lengthening at multiple speeds in order to plot their respective FL curves.
- The second experiment aims to determine the effect of intrinsic SRS on the control parameter determining the magnitude of co-contraction in the stabilisation of a musculoskeletal model, over various positive and negative stiffness positions in the FL curve.

In the simulations, an arm is attempting to hold up a ball, which is an inherently unstable configuration. The arm starts out in a position of local stability. The muscles are then excited in exactly symmetrical co-contraction, followed by a small velocity perturbation applied to the ball. No feedback system is included, so any stabilisation must come from the intrinsic muscle feedback path. The simulation is repeated while gradually lowering the applied excitation until the arm is no longer able to be stabilised by the muscles. This will be done on both a 1DoF and a 2DoF model, in order to see if the same effect will occur for a more complex musculoskeletal system. The positive stiffness position experiments should imitate a more biologically realistic experimental setup, where the muscles are free to actuate in their optimal range. The negative stiffness positions should test whether the SRS affects the control parameter in a more extreme end of the muscle range. The experiment is repeated for each muscle model.

- In the third and last experiment, the effect of intrinsic muscle stiffness on the robustness of the feedback parameters of simple individual muscle feedback systems is determined in reaching experiments similar to Flash and Hogan [13].

First, optimal feedback parameters for each muscle will be determined for each muscle model, for a set of reaching tasks. Then, the tasks will be repeated while altering the feedback parameters individually to map the parameter space. The magnitude of the effect of altered feedback parameters on task performance will be how robustness is determined.

These three experiments should illustrate the effect of intrinsic muscle stiffness on the neural control parameters.

2 METHODS

A list of all the parameters used in the various experiments is given in Appendix A.

2.1. MUSCLE MODELS

2.1.1. HILL MODEL

HILL MODEL: THEORY

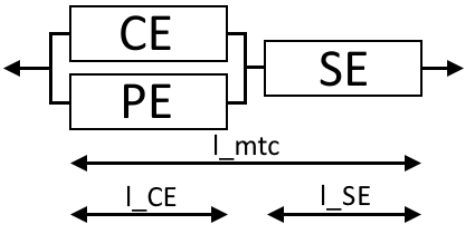

Figure 2.1.: This model simulates the muscle tendon-complex (MTC) which contains two elastic components, the parallel element (PE) and the series element (SE), as well as the contractile element (CE), which is the main source of force production[11]. This construction is the same for the Hill_expanded and the Huxley model. The Hill_simple model contains a simplified SE which stays at length l_t throughout the simulations and does not include a PE.

To simulate muscle dynamics, one must take into account a range of different behavioural phenomena. The main function of the muscle is a quick, concentric contraction as a direct result of neural stimulation. The microscopic elements in a muscle that cause this contraction are called the cross-bridges, or small molecular bonds that form between the actin and myosin strands in a muscle[34]. While these bands provide the contracting power in the muscle, they are also elastic to a certain extent. The elasticity of both the cross-bridges and the tendon that the muscle is attached to both play a significant role in muscle behaviour[24]. Lastly, the passive stiffness of a muscle increases with stretch[35].

The Hill-type model comes in many different versions which all aim to replicate the many non-linear behavioural characteristics that arise from the active and passive muscle properties. The Hill-type model generally consists of a contractile element (CE) and a series elastic element (SE), representing respectively the active muscle force and the elasticity of both the tendon and the actin-myosin cross-bridges[36][10]. The CE in the Hill model accurately describes shortening contractions in muscle, but it is less ef-

fective in describing lengthening contractions[10]. The CE FV (FV) behaviour in the original Hill [6] model is described by this hyperbolic equation for shortening muscle in Eq. 2.1:

$$(F+a)(v+b)=(f_{max}+a)b \tag{2.1}$$

Here is F the muscle tensile force and v the shortening velocity, with a and b being constants. Patterns described here are commonly found in a number of different ways. For example, many distinct chemical processes lead to the Hill equation pattern[37][27]. The Hill-type model also usually includes a parallel elastic element (PE) to model the passive muscle stiffness stemming from the muscle fibers[36]. The PE force is often negligible at normal ranges[10]. Some models also include a damping element (DE) to describe mechanical muscle behaviour [36]. Damping can also be included in the SE element [38], though the original Hill model specified an undamped SE [24]. An overview of the components of the muscle models used in this paper can be seen in Fig. 2.1.

HILL_EXPANDED: IMPLEMENTATION

The Hill_expanded model is based on Franzen [2]. To minimize the differences between this model and the Huxley model in our simulations, some changes were applied to this implementation of the Hill model. The first difference is that the PE length in this implementation is equal to the CE length, rather than the muscle-tendon complex (MTC) length. Furthermore, the used parameters were taken from the Vardy *et al.* [11] and the Stroeve [12] experiments, equal for all used muscle models. The Hill_expanded model includes explicitly calculated force-length (FL) and force-velocity (FV) relationships. The FL is a Gaussian function seen in Eq. 2.2, derived from Stroeve [12]. Here $-l_{CE_0}$ is the optimal length constant, the value of which changes for each simulation.

$$F_L(l_{CE})=e^{(-(\frac{l_{CE}-l_{CE_0}}{l_{CE_{sh}}})^2)} \tag{2.2}$$

In this equation, $l_{CE_{sh}}$ is the width of the Gaussian FL curve, calculated in Eq. 2.3.

$$l_{CE_{sh}}=l_{sh}(l_{max}-l_{min}) \tag{2.3}$$

l_{max} and l_{min} are calculated through Eq. 2.4, where $m=1..6$ refers to the muscle number, l_{rm} the resting muscle length and $r_{m1,2}$, $\alpha_{1,2}$ and $\alpha_{r1,2}$ refer respectively to the shoulder and elbow joint radii, minimum or maximum joint angles and resting joint angles. The joint ranges of the shoulder and elbow are $[0,\pi]$ and $[\alpha_1-0.1\pi,\alpha_1+0.9\pi]$.

$$l_m=l_{rm}-r_{m1}\cdot(\alpha_1-\alpha_{r2})-r_{m2}\cdot(\alpha_2-\alpha_{r2}) \tag{2.4}$$

The maximum CE velocity and the explicit FV formula are based on Winters and Stark [20] and given in Eq. 2.5 and Eq. 2.6.

$$v_{max}(a,l_{CE})=V_{vm}(1-V_{er}(1-a\cdot F_L(l_{CE}))) \tag{2.5}$$

Here, V_{vm} is a parameter determining the maximum velocity for concentric contraction.

$$F_V(v_{CE})=\begin{cases}0 & \dot{l_{CE}}\le -v_{max}\\ \frac{V_{sh}(v_{max}+\dot{l_{CE}})}{V_{sh}v_{max}-\dot{l_{CE}}} & -v_{max}<\dot{l_{CE}}\le 0\\ \frac{V_{sh}V_{shl}v_{max}+V_{ml}\dot{l_{CE}}}{V_{sh}V_{shl}v_{max}+\dot{l_{CE}}} & \dot{l_{CE}}>0\end{cases} \tag{2.6}$$

Here V_{sh} and V_{shl} are shape factors determining the concavity of the Hill-curve during contracting and lengthening, respectively[12]. V_{er} determines the effect of the activation on the maximum velocity[12].

The forces of the PE and the SE are calculated in Eq. 2.7 and Eq. 2.8.

$$F_{PE}=\frac{e^{(\frac{PE_{sh}}{PE_{xm}}\cdot l_{PE}-1)}}{e^{(PE_{sh}-1)}} \tag{2.7}$$

$$F_{SE}=\frac{e^{(\frac{SE_{sh}}{SE_{xm}}\cdot l_{SE}-1)}}{e^{(SE_{sh}-1)}} \tag{2.8}$$

Here, PE_{xm} and SE_{xm} are isometric passive and tendon strain factors.

The velocity of the CE is calculated with Eq. 2.9. f_{rel} is seen in Eq. 2.10. The f_{rel} input it changed from F_{SE} to $F_{SE}-F_{PE}$ to account for the change in the l_{PE}

$$v_{CE}=\begin{cases}\frac{V_{sh}v_{max}(f_{rel}-1)}{(f_{rel}+V_{sh})} & 0\le f_{rel}\le 1\\ \frac{V_{sh}V_{shl}v_{max}(f_{rel}-1)}{(f_{rel}+(-1-(1+V_{sh}V_{shl})(V_{ml}-1))} & 1\le f_{rel}\le V_{ml}\end{cases} \tag{2.9}$$

Here, V_{ml} is a parameter determining the maximum velocity for eccentric contraction.

$$f_{rel}=\frac{a\cdot(F_{SE}-F_{PE})}{f_{max}\cdot F_L(l_{CE})} \tag{2.10}$$

The CE muscle force is calculated in Eq. 2.11.

$$F_{CE}=a\cdot F_L(l_{CE})\cdot F_V(\dot{l_{CE}})\cdot f_{max} \tag{2.11}$$

Then the total muscle force is calculated in Eq. 2.12.

$$F_{mtc}=F_{CE}+F_{PE} \tag{2.12}$$

This muscle model was verified by checking whether Eq. 2.13 held throughout the simulation, starting at $50ms$ after excitation onset and at perturbation onset, as the CE force starts incongruent with the SE force at $\overrightarrow{v_{STIM}}=0$ and the system dynamics take some time to stabilise.

$$F_{SE}=F_{CE}+F_{PE} \tag{2.13}$$

HILL_SIMPLE: IMPLEMENTATION

The Hill_expanded includes explicit FL and FV relationships. The Hill_simple model does too, though is more simplified by including a static SE and excluding a PE. The l_{CE} and v_{CE} are calculated in Eq. 2.14 and Eq. 2.15, where l_t is the static tendon length. The other equations match the Hill_expanded model. It is implemented in the same way as in Stroeve [12], with the exception of the activation model, which is the same for all models in this paper.

$$l_{CE}=l_{mtc}-l_t \tag{2.14}$$

$$\dot{l_{CE}} = v_{CE} = \dot{l_{mtc}} \tag{2.15}$$

2.1.2. HUXLEY MODEL

HUXLEY MODEL: THEORY

The original partial differential equation introduced by Huxley [8] is given in Eq.2.16.

$$\frac{\partial n}{\partial t} - v(t)\frac{\partial n}{\partial x} = f(x) - [f(x) + g(x)]n \tag{2.16}$$

Here, the variable n is a probability distribution function representing the fraction of attached actin-myosin cross-bridges. $f(x)$, $g(x)$ and x represent the bonding, unbonding and distance from the equilibrium of said cross-bridges. They are given as applied in this paper in Eq. 2.17, Eq. 2.18 and 2.19 [10][11]. Here N is the number of cross-bridges and h is the maximum bond length. These $f(x)$ and $g(x)$ functions are given in the Vardy *et al.* [11] model, but many more variations exist.

$$f(x) = \begin{cases} 0, & x < 0 \\ f_1 \cdot (\frac{x}{h}), & 0 < x \leq h \\ 0, & x > h \end{cases} \tag{2.17}$$

$$g(x) = \begin{cases} g_2, & x < 0 \\ g_1 \cdot (\frac{x}{h}), & 0 < x \leq h \\ g_1 \cdot (\frac{x}{h}) + g_3 \cdot (\frac{x}{h} - 1), & x > h \end{cases} \tag{2.18}$$

$$\vec{x} = [x_1, x_2, .., x_N] \tag{2.19}$$

The Huxley model is often described as implicit and bottom-up[7]. This is the reason non-linear muscle phenomena such as short-range stiffness (SRS) can be readily modelled with the Huxley model. To address the issue of high computational costs associated with the Huxley model, the simplified model proposed by Vardy *et al.* [11] is used.

The Vardy *et al.* [11] model is an implementation of the method of characteristics proposed by Zahalak [39], which reformulates the original Huxley [8] model as a non-linear state-space model, which allows for easy incorporation into any large-scale musculoskeletal model and *may provide better estimates for muscle force and metabolic energy consumption*[11], at least when binding parameters are estimated from in vivo data. An overview of the model components can be seen in Fig. 2.1. Eq. 2.20 depicts the input vector, with l_{MTC} being the MTC length, v_{MTC} the velocity and $a(t)$ the activation level[11].

$$\begin{vmatrix} l_{MTC} \\ v_{MTC} \\ a(t) \end{vmatrix} \tag{2.20}$$

The state vector can be seen in Eq. 2.21 where l_{CE} being the CE length, v_{CE} the CE velocity and the cross-bridge stretch velocity $\dot{\vec{x}}$ can be derived directly from the MTC velocity vector $\vec{v}$[11][39][8].

$$\frac{d}{dt}\begin{vmatrix} l_{CE} \\ \vec{x} \\ \vec{n} \end{vmatrix} = \begin{vmatrix} v_{CE} \\ v_{\vec{MTC}} \\ (f(x) - (f(x) + g(x))\vec{n} \end{vmatrix} \tag{2.21}$$

Then, the output vector is shown in Eq. 2.22. Here the CE force F_{CE} can be calculated using only x and n as variables[11]. The n^{ss} is the steady state of $n(x,t)$ and is introduced so $F_{CE} = f_{max}$ at isometric conditions[11].

$$F_{CE} = \frac{f_{max}\int_{-\infty}^{\infty} x n(x,t)dx}{\int_{-\infty}^{\infty} x n^{SS}(x,t)dx} \tag{2.22}$$

HUXLEY MODEL: IMPLEMENTATION

The used state vector is Eq. 2.23 with k scaling with the number of cross-bridges used.

$$\overrightarrow{v_{STATES}} = [x_1 ....x_k, n_1 ....n_k, l_{ce}, act] \tag{2.23}$$

$\vec{x}$ is the cross-bridge length vector and $\vec{n}$ is the the corresponding cross-bridge distribution vector[11]. The initial state vector is determined as follows. x_0 values are obtained from a random uniform distribution of $[-30 \cdot h, 30 \cdot h]$. h here is a constant referring to the maximum cross-bridge bond length. n_0 values are calculated from their respective x_0 values using Eq. 2.24.

$$n_0(x) = \frac{f(x)}{f(x) + g(x)} \begin{cases} 0, & x < 0 \\ \frac{f1}{f1 + g1}, & 0 < x \leq h \\ 0, & x > h \end{cases} \tag{2.24}$$

x values are limited to $[-2 \cdot h, 4 \cdot h]$ in accordance to Wu, Herzog and Cole [40]. l_{ce_0} is found by Thelen [41] SE stiffness equations and is based on the $l_{ce_{opt}}$. The state vector containing muscle model-specific information was updated every time-step using the forward-Euler method. The input vector is $[v_{mtc}, l_{mtc}, \overrightarrow{v_{STIM}}]$. Here, v_{mtc} is the muscle-tendon complex (MTC) velocity, l_{mtc} is the MTC length and $\overrightarrow{v_{STIM}}$ is a parameter with range $[0,1]$ describing the level of excitation the muscle receives from neural input. This excitation is assumed to be equal for the entire muscle at once.

The stretch velocity of the cross-bridges v_{cb} is related to the stretch velocity of the CE [39][8][11]through Eq. 2.25.

$$v_{CE}(t) = \frac{2 \cdot l_{CE_{opt}}}{s} \cdot v_{cb} = \lambda \cdot v_{cb} \tag{2.25}$$

The CE velocity is calculated with Eq. 2.26 [11].

$$v_{CE} = \frac{v_{MTC} \cdot K_{SE} - f_{max} \cdot C2 \cdot (I_f(x,n) + I_H(x,n))}{K_{SE} + K_{PE} + f_{max} \cdot C2 \cdot I_n(x,n)} \tag{2.26}$$

Here, $C2$, I_n, I_f, I_H and I_x are defined in Eq. 2.33, Eq. 2.27, Eq. 2.28, Eq. 2.29 and Eq. 2.30.

$$I_n = \lambda^{-1} \cdot \int_{-2h}^{4h} n(x,t)dx \tag{2.27}$$

$$I_f = \int_{-2h}^{4h} x \cdot f(x)dx \tag{2.28}$$

$$I_H = \int_{-2h}^{4h} x \cdot -(f(x) + g(x)) \cdot n(x,t)dx \tag{2.29}$$

$$I_x = \int_{-2h}^{4h} x \cdot n(x,t)dx \tag{2.30}$$

The stiffness'K_{SE} and K_{PE} were found using Thelen [41] equations.

The CE muscle force is finally calculated using the

trapezoid method, as seen in Eq. 2.31 and Eq. 2.32.

$$F(x_k, n_k) = \int_{-2h}^{4h} (x \cdot n) dx \tag{2.31}$$

$$F_{CE} = a \cdot F_L(l_{CE}) \cdot C2 \cdot F(x_k, n_k) \tag{2.32}$$

Though the FV relationship is implicit, the FL relationship is explicitely included in Eq. 2.2, the same for all the models. The scaling variable $C2$ was introduced like in Vardy *et al.* [11] to represent steady-state conditions and remove the force magnitude dependence from the number of cross-bridges. It was defined in Eq. 2.33 using the trapezoid method similar to Eq. 2.31 but using the initial state vectors x_0 and n_0.

$$C2 = \frac{f_{max}}{\int_{-2h}^{4h} (x_0 \cdot n_0) dx} \tag{2.33}$$

The SE force F_{SE} is adapted from Vardy *et al.* [11], is originally from Thelen [41] and is given in Eq. 2.34.

$$F_{SE} = \begin{cases} \frac{f_{max} \cdot SE_{ftoe}(e^{\frac{SE_{sh} \cdot \epsilon_{SE}}{\epsilon_{toe}}} - 1)}{e^{SE_{sh}} - 1} & \epsilon_{SE} \leq \epsilon_{toe} \\ f_{max} \cdot (SE_{ftoe} + k_{lin} \cdot (\epsilon_{SE} - \epsilon_{toe})) & \epsilon_{SE} > \epsilon_{toe} \end{cases} \tag{2.34}$$

Here, F_{SE} the is represented by a function of the exponential shape factor SE_{xm} during an initial non-linear toe region and by a linear function of k_{lin} when the normalised SE elongation with respect to its slack length[11][41] ϵ_{SE}, given in Eq. 2.35, is larger than a tendon strain threshold ϵ_{toe}, given in Eq. 2.36.

$$\epsilon_{SE} = \frac{l_{SE} - l_{SE_{slack}}}{l_{SE_{slack}}} \tag{2.35}$$

$$\epsilon_{toe} = \frac{SE_{ftoe} \cdot SE_{SH} e^{SE_{SH}} SE_{xm}}{A} \tag{2.36}$$

Here, A is a factor calculated in Eq. 2.37.

$$A = SE_{ftoe} \cdot SE_{SH} e^{SE_{SH}} - SE_{ftoe} e^{SE_{SH}} + SE_{ftoe} + e^{SE_{SH}} - 1 \tag{2.37}$$

The linear factor k_{lin} is calculated in Eq. 2.38.

$$k_{lin} = \frac{A}{SE_{xm} \cdot (e^{SE_{SH}} - 1)} \tag{2.38}$$

The SE stiffness K_SE is given in Eq. 2.39.

$$K_{SE} = \begin{cases} \frac{(\frac{SE_{SH}}{\epsilon_{toe}}) \cdot f_{max} \cdot SE_{ftoe} \cdot e^{\frac{SE_{SH} \cdot \epsilon_{SE}}{\epsilon_{toe}}}}{(e^{SE_{SH}} - 1) \cdot l_{SE_{slack}}} & \epsilon_{SE} \leq \epsilon_{toe} \\ \frac{f_{max} \cdot k_{lin}}{l_{SE_{slack}}} & \epsilon_{SE} > \epsilon_{toe} \end{cases} \tag{2.39}$$

The PE stiffness is also calculated using a model from Thelen [41] like in Vardy *et al.* [11], given in Eq. 2.40.

$$K_{PE} = \begin{cases} \frac{(\frac{PE_{SH}}{PE_{xm}}) \cdot f_{max} \cdot e^{\frac{PE_{SH} \cdot \epsilon_{PE}}{PE_{xm}}}}{(e^{PE_{SH}} - 1) \cdot l_{PE_{slack}}} & \epsilon_{PE} > 0 \\ 0 & \epsilon_{PE} \leq 0 \end{cases} \tag{2.40}$$

Here, the normalised PE elongation with respect to its slack length[11][41] ϵ_{PE}, given in Eq. 2.41.

$$\epsilon_{PE} = \frac{l_{PE} - l_{PE_{slack}}}{l_{PE_{slack}}} \tag{2.41}$$

The passive PE muscle force is calculated based on Thelen [41] with Eq. 2.42. Here PE_{xm} is referred to as the passive muscle strain due to maximum isometric force, $\hat{l_{PE}}$ is the normalise PE length and PE_{sh} is a shape factor.

$$F_{PE} = f_{max} \cdot \frac{e^{PE_{sh} \cdot (\hat{l_{PE}} - 1)/PE_{xm}} - 1}{e^{PE_{sh}} - 1} \tag{2.42}$$

The total force is then calculated in Eq. 2.43.

$$F_{total} = F_{CE} + F_{PE} = F_{SE} + F_{PE} \tag{2.43}$$

This model was verified by replicating the single muscle experiments in Vardy *et al.* [11]. The accuracy of CE force calculation in that experiment was determined by the error in Eq. 2.44. In the verification experiments, the modelled accuracy was higher than in simulations from Vardy *et al.* [11].

$$F_{SE} = F_{CE} + F_{PE} \tag{2.44}$$

2.2. SUPPLEMENTARY MODELS

2.2.1. DAMPING

For experiments in 2 Degrees of Freedom (DoF) the system will be damped around the joints and is applied in the form of a passive torque, similar to Stroeve [12]. The applied torque can be seen in Eq.2.45.

$$T_{pj} = -B_j \cdot \dot{\alpha}_j - sign(\alpha_j - \theta_{rj}) \cdot \frac{T_{maxj}}{e^{(PE_{shj})} - 1} \cdot (e^{(\frac{PE_{shj}}{PE_{xmj}} \cdot abs(\alpha_j - \theta_{rj}))} - 1) \tag{2.45}$$

Here j is the joint, B_j is the joint damping, T_{maxj} the maximum joint torque, θ_{rj} the joint rest angle, PE_{shj} and PE_{xmj} are joint shape factors.

2.2.2. ACTIVATION

The activation model used is based on Raasch and Zajac [42]. The activation parameters t_{act} and t_{deact} are taken from Stroeve [12] as 40 and 70, respectively. It is assumed that the activation model choice itself will have little effect on modelling outcomes. This activation model is used with all three muscle models.

2.3. EXPERIMENT 1 PROTOCOL

Experiment 1 is designed to test hypothesis #1. This was done in three experiments, 1a, 1b and 1c. In Experiment 1a a set of forced stretches and contractions were applied to the muscle models, to produce an FL curve of the models and determine the negative stiffness region bounds were determined. In this region, a small applied stretch can experimentally result in a force increase, while a larger stretch will lead to the expected theoretical force decrease. To access whether the force increase in the local stretch response is a consequence of stiffness or damping, in Experiment 1b

a mass-spring-damper model was fit over the data of a set of small stretches. Finally, the goal of Experiment 1c was to provide an indication of the bounds of the input on the system dynamics, so the force-length-velocity (FLV) curves of the three models were plotted. In all three experiments, the muscle forces were normalised by using a maximal force constant of $f_{max} = 1$.

2.3.1. EXPERIMENT 1A

In Experiment 1a the dynamic response of a single muscle as a consequence of forced stretch and contraction was determined for each of the muscle models. The muscle was stretched and contracted at a chosen velocity of $v_{mtc} = 80mm/s$ for $24ms$. A higher or lower velocity could make the FV contribution to total muscle force larger or smaller, respectively. The starting muscle length is $l_{mtc} = 0.32m$, which is the neutral length of the bi-articular muscles in Stroeve [12]. The optimal CE length was set at $l_{CE_{opt}} = 267.16mm$ while the starting CE length was set at $l_{CE_0} = 266.78mm$, so the muscle started slightly into the positive stiffness region of the FL curve. Then, to get a qualitative force response indication of the models responding to a local stretch in the negative stiffness region, a slower and shorter stretch was applied at a velocity of $v_{mtc} = 8mm/s$ for $14ms$, starting slightly into the negative stiffness region of the FL curve. In Fig. 2.2 an overview is seen of the applied stretches and contractions, as well as the input to the muscles which was $\overrightarrow{v_{STIM(t=0s)}} = 0$ and $\overrightarrow{v_{STIM(t>=0.5s)}} = 1$. The slow stretch was to be highlighted and zoomed in on and followed by a longer period of rest to allow the muscles to reach steady state conditions.

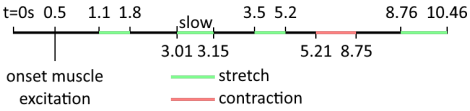

Figure 2.2.: This figure depicts the timeline of the applied muscle stretches, contraction and excitation for Experiment 1a, not to scale.

The experiment further aimed to reproduce the FL curves for each of the models. The muscle parameters exactly mirror the ones used in the Vardy *et al.* [11] and the Stroeve [12] experiments and are the same for all muscle models. The only exception is the SE_{xm} parameter, which was changed for all models from 0.04 to 0.06, to produce valid results for the Hill_expanded model, as the value of 0.04 produced SE force responses magnitudes higher and without following a known pattern. The Huxley model used 15.000 cross-bridges in this experiment, which is five times the amount used in the Vardy *et al.* [11] experiments. While muscle force normally increases with the number of cross-bridges, the scaled force in the [11] model means more cross-bridges should only increase accuracy.

2.3.2. EXPERIMENT 1B

The goal of Experiment 1b was to investigate the nature of the positive stiffness responses to a small stretch in the negative stiffness region of the FL curve. To be able to distinctly define the positive local force response as SRS or simply as a fast force increase, a distinction was made between intrinsic stiffness and intrinsic camping. It was then investigated whether the local force responses were predominantly caused by intrinsic stiffness or by intrinsic damping. The simulations were run seven times, where the only difference was the velocity and duration of the applied smaller stretch at $t = 2.01s$. The velocities were 2.0, 2.4, 2.8, 3.2, 3.6, 4.0 and $4.4mm/s$. Higher speeds would lead to a larger length and thus a change in muscle location on the FL curve, which means no analysis of a local response could have been made. The duration's were shortened to keep the stretch at a constant length of $0.4mm$ throughout the simulations. The response was split into 20 segments of equal length difference in order to investigate the origin of the force response over time. The resulting values were fitted to Eq. 2.46.

$$\delta F_{mtc} = k \cdot \delta l_{mtc} + b \cdot \delta v_{mtc} + m \cdot \delta a_{mtc} \tag{2.46}$$

Here, the stiffness k and the damping b were the variables of interest. Because the acceleration a_{mtc} was 0 throughout the experiment, the mass m could be ignored. The input to the muscles was $\overrightarrow{v_{STIM(t=0s)}} = 0$ and $\overrightarrow{v_{STIM(t>=0.5s)}} = 1$. The initial stretch of $v_{mtc} = 80mm/s$ was applied at $t = 1.1s$ to allow the muscles to reach full isometric contraction beforehand. The muscle was held at a constant length from $t = 1.5s$ until $t = 2.01s$ to achieve steady-state conditions before the smaller stretch was applied at $t = 2.01s$. The muscle parameters exactly mirror the ones used in the Vardy *et al.* [11] and the Stroeve [12] experiments and are the same for all muscle models.

2.3.3. EXPERIMENT 1C

In Experiment 1c, the goal was to plot the force-length-velocity (FLV) curves for each of the muscle models to enable a comparison between them, which should give an indication of the upper limits of velocity where the model results are similar. This was accomplished by recreating Experiment 1a, but varying the velocity and plotting the resulting FL curves next to each other. The muscles all started at the same point as in Experiment 1a with the l_{CE} slightly under the $l_{CE_{opt}}$. A long forced stretch of constant velocity was then applied, followed by a longer contraction and a subsequent stretch back to the original position. This was repeated multiple times to allow for the plotting of the curve for all the models. The duration of the applied velocity was scaled by the same factor as the velocity itself to keep the length changes equal. The upper bound of the muscle lengths l_{mtc} was also increased to demonstrate the effect of the PE force on the total muscle force. Another change to Experiment 1a is that the small stretch was removed from the simulations, though the starting lengths remained the same. The starting length of the muscles was set at $0.32m$, which is the neutral length of the bi-articular muscles in Stroeve [12]. The optimal CE length was set at $l_{CE_{opt}} = 280.00mm$ while the starting CE length was set at $l_{CE_0} = 296.78mm$. As a result, the muscles started in the negative stiffness region of the FL curve.

2.4. EXPERIMENT 2 PROTOCOL

The purpose of Experiment 2 is to test hypothesis 2 and aims to determine the effect of intrinsic SRS on the control parameter determining the magnitude of co-contraction in the stabilisation of a musculoskeletal model, over various positive and negative stiffness positions in the FL curve. This was accomplished in two parts, in experiments 2a and 2b, which are musculoskeletal systems of 1 and 2 Degrees of Freedom

(DoF), respectively. A system overview of Experiments 2.a, 2.b and 3.a is given in Fig. 2.3.

In the simulations, an arm is attempting to hold up a ball-shaped mass against gravity, which is an inherently unstable configuration. The mass is ball-shaped to simulate a moment of inertia. The arm starts out in a position of unstable equilibrium. The muscles are then excited in exactly symmetrical co-contraction, followed by a small velocity perturbation applied to the ball. No feedback system is included, so any stabilisation must come from the intrinsic muscle feedback path. The simulation is repeated while gradually lowering the applied excitation $\overrightarrow{v_{STIM}}$ until the arm is no longer able to be stabilised by the muscles. The test variable of this experiment was the lowest level of excitation $\overrightarrow{v_{STIM}}$ required to stabilise the system using only the co-contraction strategy of the two muscles in a forward dynamic simulation.

The system was considered to be stable when both of the following conditions were met. 1: The mass position deviated no more than $0.001m$ from the neutral position. 2: The net joint angular velocity $\dot{\alpha}$ of the joint controlling the limb attached to the ball could not be positive in the direction away from the neutral position after at most $10s$. It is assumed that this chosen stability definition should allow for valid comparison when consistently used. In all experiments, the muscles were first activated at $t = 0.1s$ while the system was still in the neutral position, where all joint angles are equal to $\alpha = 0.5 \cdot \pi rad$ and the angular velocities equal to 0. A perturbation is then applied in the shape of angular velocity $\dot{\alpha} = 0.005 \cdot \pi rad/s$ at $t = 0.25s$, in order to activate the FV response of the muscles and to bring the system out of a local stability position.

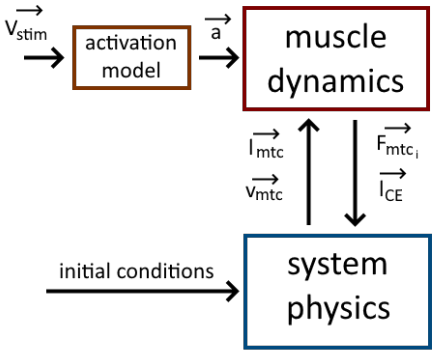

Figure 2.3.: This figure depicts what the exchange of values per timestep looks like on a system-level, simplified. The system physics is calculated through the TMT method combined with a runga kutta 4 integrator in experiments 2.a, 2.b and 3.a. The initial conditions are an initial position and velocity for each generalised coordinate. The only external input to the system besides the initial conditions is a vector $\overrightarrow{v_{STIM}}$ containing the levels of excitation for each muscle. This vector is subsequently fed through a first-order model into levels of muscle activation at each time step. Both parameters are bounded at [0,1].

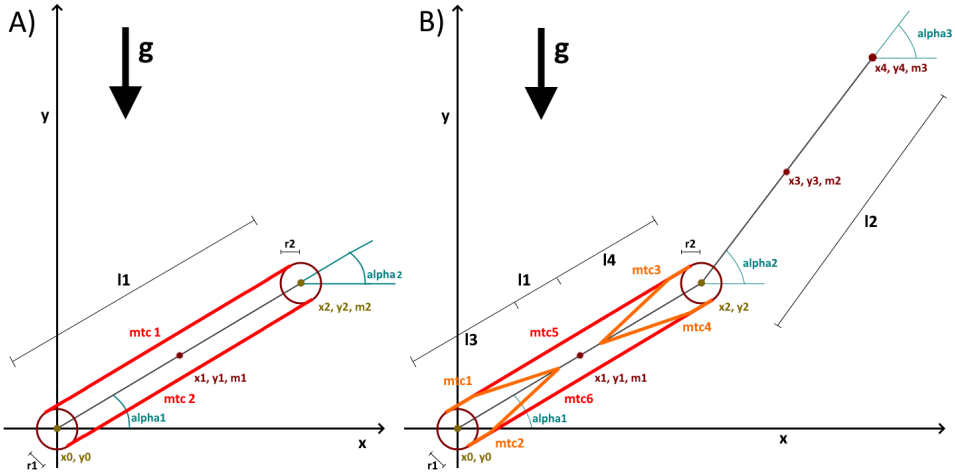

Figure 2.4.: Both figures depict a testbed adapted from the Stroeve [12] model used in Experiment 2. All muscles are assumed to apply a torque equal to the muscle force times the joint radius $T_{MTC} = F_{MTC} \cdot r_{joint}$. The joint radius is taken from Stroeve [12]. The contraction direction is the assumed force vector. (A) The testbed from Experiment 2A. The locations of the system coordinates x_{0-2}, y_{0-2} as well as the generalised coordinates $[\alpha_1, \alpha_2]$ are shown. The second generalised coordinate α_2 is added to represent the held mass m_2 at the distal end of the limb. (B) The testbed from Experiment 2B. The locations of the system coordinates x_{0-4}, y_{0-4} as well as the generalised coordinates $[\alpha_1, \alpha_2, \alpha_3]$ are shown. The third generalised coordinate α_3 is added to represent the held mass m_3 at the distal end of the limb. For the bi-articular muscles 5 and 6, the muscle connections at the joint rotate along with the joint.

Three models are compared, the Huxley model, the Hill_expanded model, and the Hill_simple model. The series of simulations were performed five times with one of five optimal contractile elements (CE) lengths $l_{CE_{opt}}$ and starting CE lengths l_{CE_0}. A positive difference indicates that the muscles'starting position is left of the peak in the FL curve, which defines the positive stiffness region of the curve. This was done to investigate the effects of the FL locality on the stabilisation. Because the range of successful stabilisation is defined as small relative to the range of the musculoskeletal system, any observed stabilising muscle behaviour occurs completely within the predefined stiffness region of the FL curve, isolating the results to the region. The differences between these values $l_{CE_{opt}} - l_{CE_0}$ were in the order from high positive to high negative $34.9mm$, $19.4mm$, $3.8mm$, $-11.8mm$ and $-27.3mm$ for the muscles in Experiment 2a and for the bi-articular muscles 5 and 6 in Experiment 2b. For the smaller muscles 1-4 in Experiment 2b, these differences were set at $43.9mm$, $28.3mm$, $12.8mm$, $-2.8mm$ and $-18.3mm$. These values were chosen so the differences all differ exactly $15.561m$ from each other. A visual overview of the stiffness regions is given in Fig. 3.4. In both experiments, a gravitational constant of $g = 9.81m/s^2$ is used.

2.4.1. 2A: 1DOF

Experiment 2A used a 1DoF system with two muscles, partially modelled after the Stroeve [12] model. The configuration for the musculoskeletal system used is depicted in Fig. 2.4. The system dynamics were calculated using the TMT method. The system started in a locally stable position with the initial conditions for the generalised coordinates being set at $[\alpha_1, \alpha_2, \dot{\alpha_1}, \dot{\alpha_2}] = [0.5 \cdot \pi rad, 0, 0, 0]$. At $t_{stim} = 0.1s$ the co-contraction started through the application of excitation equal to $1 \cdot \overrightarrow{v_{STIM}}$. The perturbation was applied at $t_{pert} = 0.25s$. The perturbation consisted of the following perturbation vector being added to the current system variables $\vec{v_{pert}} = [\delta\alpha_1, \delta\alpha_2, \delta\dot{\alpha_1}, \delta\dot{\alpha_2}] = [0.005 \cdot \pi rad \cdot s^{-1}, 0, 0, 0]$. Values for r_1, r_2, l_1 and m_1 were set at $0.03m$, $0.03m$, $0.32m$ and $1.8kg$, respectively. The proximal ends of the muscles were fixed at the starting position of the shoulder to make them function as mono-articular. The ball object at x_2, y_2 was defined as a circle with mass $m_2 = 1kg$ and a moment of inertia $J2 = 0.0008kg \cdot m^2$.

2.4.2. 2B: 2DOF

Experiment 2B used a 2DoF system with six muscles, modelled after the Stroeve [12] model. All relevant constants are directly copied. The configuration for the musculoskeletal system used is depicted in Fig. 2.4. The system dynamics were calculated using the TMT method. The system started in a locally stable position with the initial conditions for the generalised coordinates being set at $[\alpha_1, \alpha_2, \alpha_3, \dot{\alpha_1}, \dot{\alpha_2}, \dot{\alpha_3}] = [0.5 \cdot \pi rad, 0.5 \cdot \pi rad, 0, 0, 0, 0]$. At $t_{stim} = 0.1s$ the co-contraction started through the application of excitation equal to $1 \cdot \overrightarrow{v_{STIM}}$. The perturbation was applied at $t_{pert} = 0.25s$. The perturbation consisted of the following perturbation vector being added to the current system variables $\vec{v_{pert}} = [\delta\alpha_1, \delta\alpha_2, \delta\alpha_3, \delta\dot{\alpha_1}, \delta\dot{\alpha_2}, \delta\dot{\alpha_3}] = [0, 0.005 \cdot \pi rad \cdot s^{-1}, 0, 0, 0, 0]$. The ball object at x_4, y_4 was defined as a circle with mass $m_3 = 1kg$ and a moment of inertia $J2 = 0.0008kg \cdot m^2$.

2.5. EXPERIMENT 3 PROTOCOL

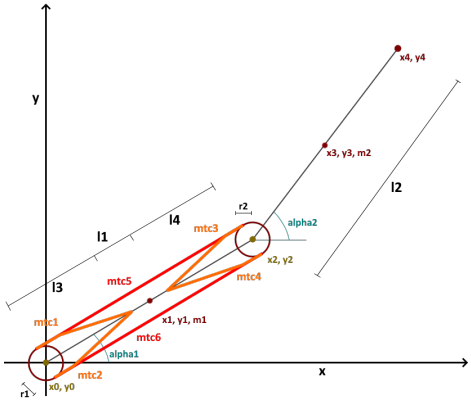

Figure 2.5.: Exp 3: The testbed adapted from the Stroeve [12] model has two degrees-of-freedom (DoF) and includes six muscles. For the bi-articular muscles 5 and 6, the muscle connections at the joint rotate along with the joint. All muscles are assumed to apply a joint torque equal to the muscle force times the joint radius $T_{MTC} = F_{MTC} \cdot r_{joint}$. The joint radii are taken from Stroeve [12]. The contraction direction is the assumed force vector. The forces of muscles are applied as torques at the joints. The locations of the system coordinates x_{0-4}, y_{0-4} as well as the generalised coordinates $[\alpha_1, \alpha_2]$ are shown.

The goal of Experiment 3 was to evaluate the parameter spaces of the feedback parameters of individual muscle feedback parameters in reaching movements, allowing for a comparison of the feedback parameter robustness between the muscle models. For this experiment, a simple reflex feedback system was applied to all muscles individually. All constants that are not already defined in Vardy *et al.* [11] are directly copied. The configuration for the musculoskeletal system used is depicted in Fig. 2.5. The system dynamics were calculated using the TMT method. The reaching task was implemented similarly to Flash and Hogan [13]. The optimal trajectories for reaching trajectory 3 from Flash and Hogan [13] are compared to the optimised trajectories created using the feedback system in the Huxley and the Hill_expanded models. Only trajectory 3 was chosen, similar to experiments by Shadmehr and Mussa-Ivaldi [43]. The optimal CE length l_{CE_0} was chosen so the muscles started in the negative stiffness region. The musculoskeletal system in Experiment 3 is almost the same as the one used for Experiment 2, with the key difference being the gravity. While the musculoskeletal system in Experiment 2 works against gravity in the coronal plane, in Experiment 3 the arm is performing reaching movements horizontally in the transversal plane. As the calculations are made in only two dimensions, the gravity force field is negated in this experiment.

2.5.1. FEEDBACK SYSTEM

The feedback system was created specifically for this experiment and has an arbitrary structure. The input vector is given in Eq. 2.47.

$$[l_{mtc}, v_{mtc}, l_{mtc_{opt}}, v_{mtc_{opt}}, \overrightarrow{v_{fb}}, \overrightarrow{v_{STIM_i}}] \tag{2.47}$$

Here, $\overrightarrow{v_{fb}}$ is a vector containing 4 feedback parameters. $\overrightarrow{v_{fb}}$ is equal for all the muscles. $l_{mtc_{opt}}$ and $v_{mtc_{opt}}$ are derived from the optimal trajectories found in experiments from Flash and Hogan [13]. The output of the feedback system is an adjusted excitation parameter $\overrightarrow{v_{STIM_{i+1}}}$. It is calculated in Eq. 2.48.

$$\begin{aligned}\overrightarrow{v_{STIM_{i+1}}} &= a \cdot (l_{mtc} - l_{mtc_{opt}}) \\ &+ b \cdot (v_{mtc} - v_{mtc_{opt}}) + c \cdot (\overrightarrow{v_{STIM_i}}) + d\end{aligned} \tag{2.48}$$

The output excitation $\overrightarrow{v_{STIM_{i+1}}}$ was limited at $[0.05, 1]$. The lower limit was put in place to avoid the optimiser from finding unrealistic local optima for $\overrightarrow{v_{fb}}$ where most muscles are not at all activated.

The optimal values for the parameters in $\overrightarrow{v_{fb}}$ were found using a standard genetic optimisation algorithm for each of the muscle models. This algorithm was chosen due to its flexibility, the fact that the $\overrightarrow{v_{fb}}$ only has a dimension of 4 which suits it well and the fact that the simulations were black box simulations where no analytical gradient could be computed. The cost function C for the optimisation was defined as the squared trajectory error of the end-point integrated over the trajectory, given in Eq. 2.49.

$$C = \int_{t_0}^{t_f} \left(\sqrt{x_4^2 + y_4^2} - \sqrt{x_{4_{opt}}^2 + y_{4_{opt}}^2} \right)^2 dt \tag{2.49}$$

Here, t_0 and t_f are the start- and endpoints of the experiment, set at 0 and 0.35 respectively to allow for the same duration as the Flash and Hogan [13] experiments. x_{4opt} and y_{4opt} are the optimal values for x_4 and y_4.

2.5.2. EVALUATION OF ROBUSTNESS

Robustness of the parameters in $\overrightarrow{v_{fb}}$ was defined here as the inverse of the degree to which a change in variables negatively affected the reaching task. To allow for the plotting of the parameter spaces, the feedback parameters were individually scaled over a range of $[-50\%, +50\%]$ in steps of 5%. If the cost function changed more as a consequence of the scaling of a feedback parameter then the parameter was considered less robust than vice versa.

3 RESULTS

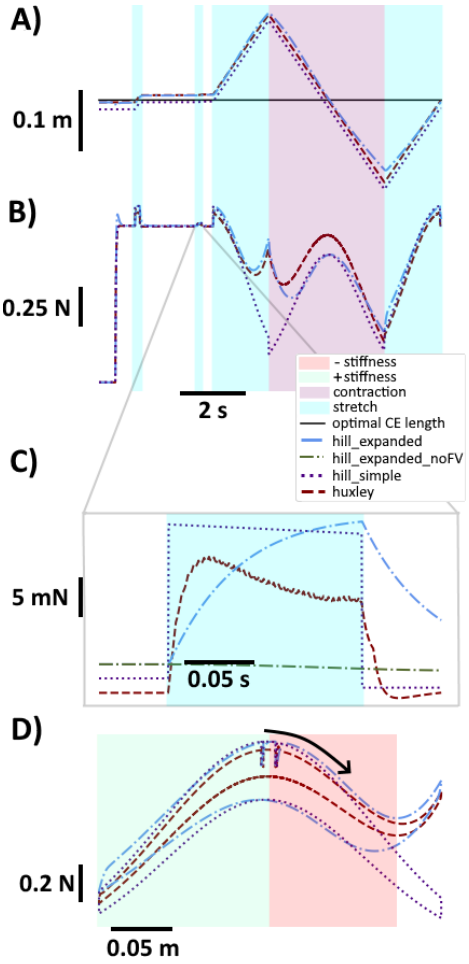

Figure 3.1.: Exp 1A: The response of the models to applied forced stretches and contractions of $80 mm/s$. (A) The applied stretch and contraction to the contractile elements (CEs) for the Hill_expanded, the Hill_simple and the Huxley models. (B) The resulting force-time plots. The gray lines indicate the region where the small stretch of $8 mm/s$ was applied. (C) The zoomed force-time plot of the small stretch in 2. (D) The force plotted directly against the muscle length. The black arrow indicates the start and direction of the plot over time. The stiffness regions of the FL curve are highlighted. The two lower forces around the beginning are the beginning of stretches.

3.1. EXPERIMENT 1

3.1.1. EXPERIMENT 1A

The applied stretch to the CEs of the models is depicted in Fig. 3.1.1. The resulting force-time plot can be seen in Fig. 3.1.2. The FL curve is produced by plotting the produced force against the corresponding muscle lengths from the simulation. The resulting FL curves are depicted in 3.1.4.

The region left from the FL peak is considered the positive stiffness region, as an increase in length here corresponds to an increase in produced force. The region right from the curve peaks is considered the negative stiffness region. At $t = 2.01s$, a small stretch is applied. The force-response is depicted in 3.1.3. This is plotted for all the models, as well as once for the Hill_expanded model without including the explicit FV model in the simulations, which depicts no positive stiffness effect whatsoever. This illustrates that without an explicit FV, which is included in both the Hill_expanded and the Hill_simple models, no positive stiffness behaviour can arise in the negative stiffness region of the FL curve. On the contrary, the Huxley model that does not include an explicit FV model indeed shows a force increase throughout the stretch, peaking right at the beginning. It is expected that this initial peak is what is referred to as the SRS. Furthermore, the Hill_expanded model l_{CE} is consistently higher at lengths away from the optimal length $l_{CE_{opt}}$. This causes higher PE forces. Lastly, it can be observed that while stretch forces are similar across the models, the Huxley model produces higher forces during contraction above a muscle length of $l_{mtc} = 0.25m$.

3.1.2. EXPERIMENT 1B

Fig. 3.2 depicts the analysis of responses to the small stretches applied in the negative stiffness region of the FL curve. Fig. 3.2. (middle) shows that the Huxley model displays a higher stiffness in the segments leading up to and including the force peak, segments 0-5. This stiffness then slowly trends to negative in subsequent segments, which corresponds to a decelerated force decrease from the peak onward. The Hill_expanded model depicts a more delayed stiffness increase that peaks at $0.104N/m$. The Huxley model displays a peak stiffness of $0.414N/m$, which is 296.53% higher than the maximum stiffness in the Hill_expanded model. The Hill_simple model only shows a negative stiffness for all of the segments.

Fig. 3.2.(C) shows that while the Huxley model displays higher damping in the first segment, this quickly becomes negative in subsequent segments, followed by a steady-state damping of around $0Ns/m$. The Hill_expanded model depicts an initial peak of $41.52Ns/m$, followed by a continuously decreasing damping, reaching a steady state of slightly below $0Ns/m$. The Huxley model displays a peak damping of $115.76Ns/m$, which is 178.79% higher than the maximum stiffness in the Hill_expanded model. Again, the Hill_simple model only shows negative damping for all of the segments and will be excluded from the comparison. The lack of damping or stiffness variation in the Hill_simple model can be attributed to the static nature of the v_{CE} calculation, where the v_{mtc} is taken directly, which means the response to static velocity is constant.

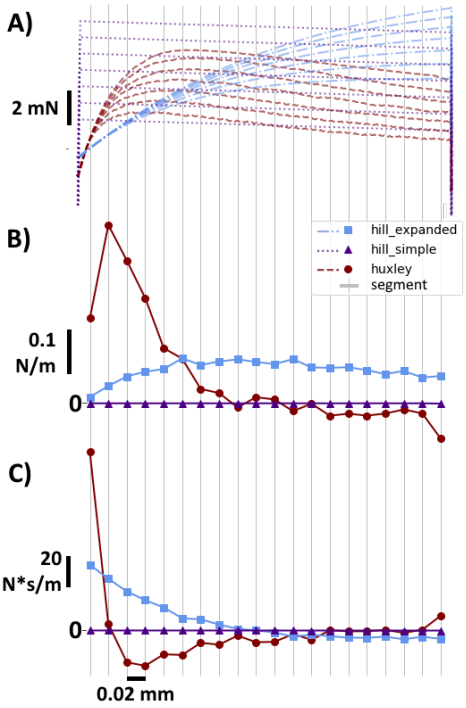

Figure 3.2.: Exp 1B: The analysis of the responses to a small stretch applied in the negative stiffness region of the force-length curves for all the models is depicted in three parts. (A) The force-time plot depicts the force response to a small stretch of $2.4mm/s$ with an $f_{max} = 1$. The response is divided into 20 segments of equal length. (B) The fitted stiffness values are plotted for each segment of each model. (C) The fitted damping values plotted for each segment of each model.
The stiffness and damping coëfficient for each segment have fitted using data from seven different velocity simulations. The velocities were 2.0, 2.4, 2.8, 3.2, 3.6, 4.0 and $4.4mm/s$. As the force velocity (FV) component of the hill1_simple model generates force instantly, the relative damping and stiffness at the start and end of the segments are disproportionally high. As a result The first and last segment start and end respectively at 1 frame into the start and end of the movement itself to be able to compare the models.

The stiffness of the Huxley model is higher than the Hill_expanded model in the first 5 segments, amounting depending on the velocity to between ~ 23 and ~ $50ms$, is consistent with experimental findings on the SRS duration from Franzen [2], which appears to be anywhere between 25 to $45ms$. In experiments from Van Eesbeek *et al.* [44], SRS windows of likewise $40ms$ are used for parameterisation.

This suggests that the increase in force production in only the Huxley model is indeed consistent with the SRS phenomenon. Furthermore, it adds to the suggestion that the apparent SRS in the Huxley model is a result of the intrinsic

muscle stiffness itself, rather than a result of the intrinsic viscosity.

3.1.3. EXPERIMENT 1C

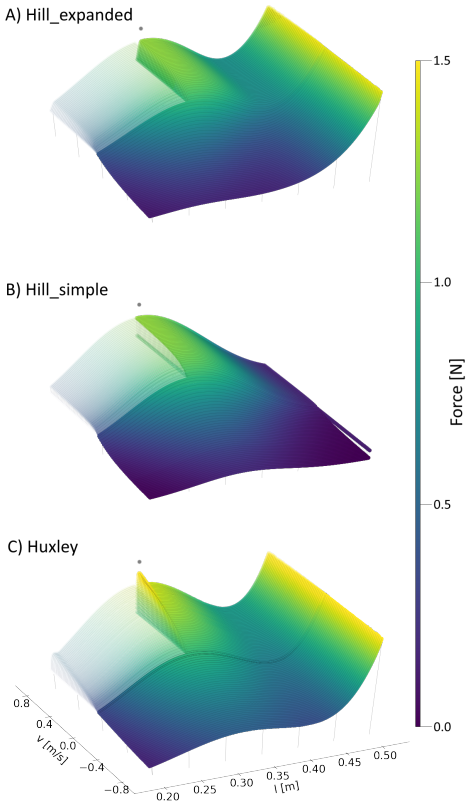

Figure 3.3.: Exp 1C: The force-length-velocity curves of the Hill_expanded model (A), the Hill_simple model (B) and the Huxley model(C). Values for one velocity are obtained by first stretching the simulated muscle from the origin around the optimal length in the middle (indicated by a grey dot), followed by concentric contraction, followed by another stretch back to the origin. The individual simulations are depicted as thin grey lines over the plot. The opacity of the plot of the final stretch back to the origin is reduced, in order to highlight the initial stretch. The simulation was repeated for a multitude of velocities, ranging from -0.8 to $0.8 m/s$.

The FLV curves of all the models are given in Fig. 3.3. It is apparent that the models all produce similar shapes in their curves, with a few key noticeable differences. The first obvious difference is the existence of relatively high peaks at the highest lengths in the Huxley and the Hill_expanded model, though they are higher for the Huxley model. Because no peaks are apparent in the Hill_simple model, the root cause of these peaks is the PE force calculations, which become higher at high lengths relative to the optimal length l_{CEopt}. Fig. 3.1.1 shows that the Hill_expanded model has a slightly higher l_{CE} upper bound, which is consistent with slightly lower PE forces. The second observation is that the Huxley model displays a much higher force during contractions. This effect becomes stronger at higher velocities, while the opposite trend holds true for the Hill-type models.

Furthermore, the Huxley model shows abnormalities in the form of higher forces at the start of the eccentric contractions, increasing with the velocity. The strongest effect can be seen right under the grey dots in Fig. 3.3. The abnormal forces could be explained by the SRS phenomenon, where the muscle force increases at the beginning of movements. The fact that the abnormalities get more pronounced at higher speeds, where the total stretch time is shorter, is additional evidence for the root cause being the SRS. These abnormalities only appear at the start of lengthening movements, but not at the start of contracting movements. This can be explained by the contracting movements starting in a range where the force production is dominated by the PE force, which overshadows the SRS effect that stems from the CE force. The abnormalities indicate that the SRS has a strong effect on forces produced at higher velocities.

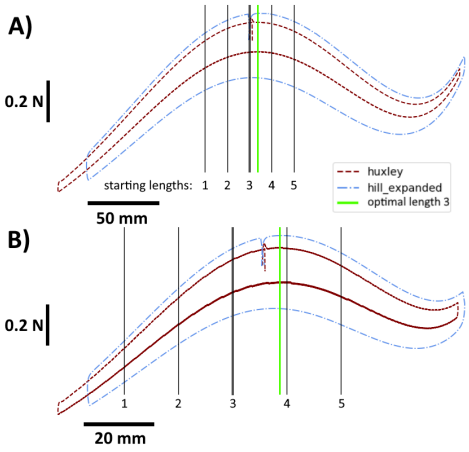

Figure 3.4.: Exp2: The stiffness regions visualised for the long muscle (A) and the short muscle (B). On the force-length (FL) curve associated with the contractile element (CE) of starting length 3, the CE starting lengths l_{CE_0} relative to the optimal lengths $l_{CE_{opt}}$ of all stiffness regions shown in Tab. A.3 are plotted. $l_{CE_{opt_3}}$ is highlighted for both muscles. The Hill_simple model is excluded for clarity. The l_{CE_0} is calculated as a function of the $l_{CE_{opt}}$ like in Thelen [41] and changes slightly for each stiffness region. The stiffness regions are all defined such that the relative difference $l_{CE_{opt}} - l_{CE_0}$ increases in steps of $15.561 mm$ for both the long and the short muscle. The stiffness regions with associated starting lengths are the following: 1. high positive, 2. medium positive, 3. low positive, 4. low negative, 5. high negative.

3.2. EXPERIMENT 2

3.2.1. EXPERIMENT 2A

The activation levels required to stabilise the system are depicted in Fig. 3.5. It is found that the Huxley model appears to need a lower level of stimulation to achieve stability using co-contraction than both Hill-type models, which is in accordance with hypothesis 2. This holds true for all cases where the Hill-type models were able to stabilise the system at all. The Hill-type models were only able to achieve stability in the high positive and the medium positive regions. In the high positive stiffness region, the Huxley model required 44.16% and 62.60% less excitation than the Hill_expanded and the Hill_simple models, respectively. For the medium positive stiffness region, the Huxley model required 46.25% and 64.75% less excitation than the Hill_expanded and the Hill_simple models, respectively.

Figure 3.5.: Exp 2A: The lowest level of activation required to stabilise the system depicted in Fig. 2.4.A using only the co-contraction strategy of the two antagonistic muscles in a forward dynamic simulation. Three models are compared, the Huxley model (left), the Hill_expanded model (middle) and the Hill_simple model (right). For each muscle model, the test was run with one of five different optimal contractile elements (CE) lengths $l_{CE_{opt}}$ and starting CE lengths l_{CE_0}. The differences between these values $l_{CE_{opt}} - l_{CE_0}$ were in the order from high positive to high negative $34.9mm$, $19.4mm$, $3.8mm$, $-11.8mm$ and $-27.3mm$. The relative locations of the stiffness regions are depicted in Fig. 3.4. A positive difference indicates that the muscles'starting positions are left of the peak in the force-length (FL) curve, which defines the positive stiffness region of the curve. For various stiffness regions of the Hill-type models, no co-contraction levels allowed for stabilisation, indicated by a red cross.

Furthermore, it was found that all of the models required a lower level of excitation to stabilise the system if the region is more positive. The Huxley model needed 13.95% more excitation in the medium positive relative to the high positive stiffness case. This was 70.13% and 73.75% for the Hill_expanded and Hill_simple models. The Huxley model was able to achieve stabilisation in all cases. The Huxley model needed 90.70% more stimulation in the high negative relative to the high positive stiffness case.

In addition to that, it was observed that both Hill-type models responded to the initial perturbation with a sharp peak in muscle velocity and muscle force, followed by a steady decline in muscle velocity resembling an inverse exponential pattern. After the peak, the joint angle moved either slowly back to the initial position or showed a slow and continued increase in activation levels where stability could not be achieved. In contrast to this, the Huxley model in stable configurations displays continued oscillations in muscle force, muscle velocity and in joint angle. For higher activation levels, though the amplitude of the oscillations is relatively small, the joint angle never returns completely to the initial position. This further suggests that the FL relationship of the Huxley model plays a relatively small role in determining the stable position of the arm. The Hill-type models did depict oscillations but over time periods at least two magnitudes larger than the periods of Huxley oscillations.

3.2.2. EXPERIMENT 2B

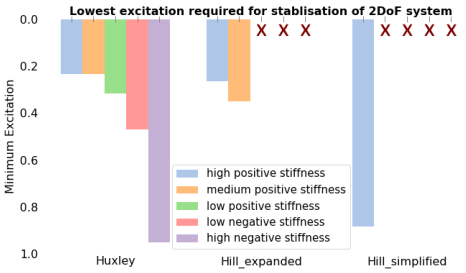

Figure 3.6.: Exp 2B: The lowest level of activation required to stabilise the system depicted in Fig. 2.4.B using only the co-contraction strategy of the six muscles in a forward dynamic simulation. Three models are compared, the Huxley model (left), the Hill_expanded model (middle) and the Hill_simple model (right). For each muscle model, the test was run with one of five different optimal contractile elements (CE) lengths $l_{CE_{opt}}$ and starting CE lengths l_{CE_0}. The differences between these values $l_{CE_{opt}} - l_{CE_0}$ were in the order from high positive to high negative $34.9mm$, $19.4mm$, $3.8mm$, $-11.8mm$ and $-27.3mm$ for the bi-articular muscles 5 and 6. For the smaller muscles 1-4 these differences were set at $43.9mm$, $28.3mm$, $12.8mm$, $-2.8mm$ and $-18.3mm$. The relative locations of the stiffness regions are depicted in Fig. 3.4. A positive difference indicates that the muscles'starting position is left of the peak in the force-length (FL) curve, which defines the positive stiffness region of the curve. For various stiffness regions of the Hill-type models, no co-contraction levels allowed for stabilisation, indicated by a red cross.

The activation levels required to stabilise the system are depicted in Fig. 3.6. It is found that the Huxley model appears to need a lower level of stimulation to achieve stability using co-contraction than both Hill-type models, which is in accordance with hypothesis 2. This holds true for all cases where the Hill-type models were able to stabilise the system at all. The Hill_expanded model was only able to achieve stability in the high positive and the medium positive regions. The Hill_simple model was only able to achieve stability in the. In the high positive stiffness region, the Huxley

model required 18.87% and 75.71% less excitation than the Hill_expanded and the Hill_simple models, respectively. For the medium positive stiffness region, the Huxley model required 30.00% less excitation than the Hill_expanded model.

Furthermore, it was found that all of the models with two or more successful stabilisation regions required an equal or lower level of excitation to stabilise the system if the region is more positive. The Huxley model needed the same level of excitation in the medium positive relative to the high positive stiffness case. This was 32.08% for the Hill_expanded model. The Huxley model was able to achieve stabilisation in all cases. The Huxley model needed 304.25% more stimulation in the high negative relative to the high positive stiffness case.

3.3. EXPERIMENT 3

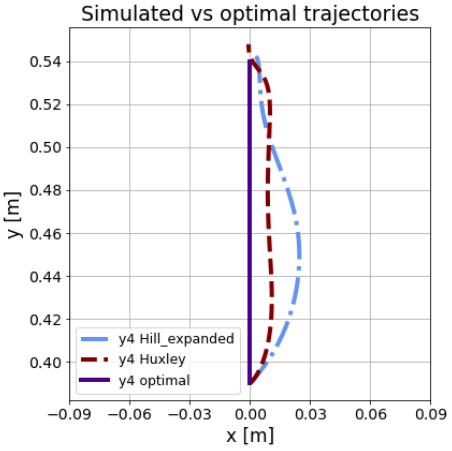

Figure 3.7.: Exp 3: The optimal trajectories for reaching trajectory 3 from Flash and Hogan [13] are compared to the optimised trajectories created using the feedback system in the Huxley and the Hill_expanded models.

The optimal and optimised simulated trajectories are depicted in Fig. 3.7. The optimised trajectory of the Huxley model more closely follows the optimal trajectory than the Hill_expanded model. This follows as the minimal costs C pertaining to them were equal to 0.0056 and 0.01114 for the Huxley and the Hill_expanded model, respectively. The found optimal feedback vectors that corresponded to these costs were $\overrightarrow{v_{fb_{opt}}} = [64.6333, 9.2010, -1.2370, 0.1285]$ and $\overrightarrow{v_{fb_{opt}}} = [82.2720, 13.7692, -0.7620, -0.0102]$ for the Huxley and the Hill_expanded model, respectively. No optimum was found for the Hill_simple model.

The parameter space of the feedback parameters relative to the cost function is depicted in Fig. 3.8. It was found that the Huxley model cost was more robust to the changing of the feedback parameters pertaining to the muscle length and velocity error parameters a and b. The Hill_expanded model, however, was more robust to the changing of the feedback parameter pertaining to the current excitation c and the dimensionless feedback parameter d. It should be noted that for both models in absolute terms, the parameters a and b were at least one magnitude larger than parameter c and at least two magnitudes larger than parameter d. Consequently, the effect parameters a and b on the production of the excitation patterns required to produce the trajectory is assumed dominant. As a result, it is stated that the Huxley model cost was more robust to the changing of the feedback parameters that are dominantly responsible for the trajectory.

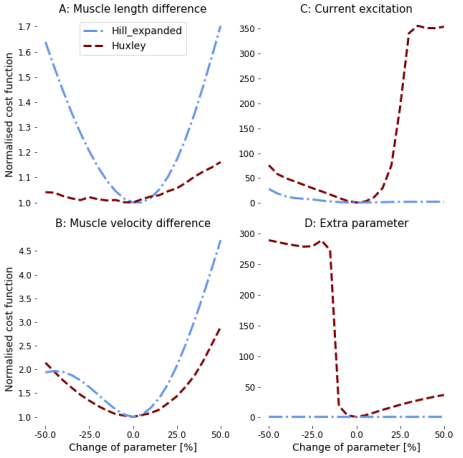

Figure 3.8.: Exp 3: The parameter space is depicted of the analysis of the responses to a small stretch applied in the negative stiffness region of the force-length curves for all the models is depicted in three parts. Optimal values were found for an arbitrary feedback system using a genetic algorithm. The feedback function works at an individual muscle level, though the feedback parameters are shared by all the muscles. It has an input vector consisting of the current excitation level, current muscle length, current muscle velocity, optimal muscle length and optimal muscle velocity. The optimal system trajectory is taken from Flash and Hogan [13] data, for reaching task 3. The system parameters were taken directly from Stroeve [12]. The output is a new excitation level, based on a parameter determining the influence of muscle length error (A), muscle velocity error (B), current excitation (C) and added extra excitation (C). The change of the normalised cost function is plotted against the change of feedback parameters. The dominant two variables were highlighted with a red exclamation mark.

4 Conclusion

The main goal of this thesis was to test how intrinsic muscle model stiffness complexity affects the magnitude of the control parameters responsible for feed-forward stabilisation and robustness of the feedback parameters influencing reaching movements in a musculoskeletal testbed. This was accomplished by stating three hypotheses and designing three experiments to test these hypotheses.

The key conclusions of this paper are the following:

- Only the Huxley model can show a positive stiffness in response to local stretch in the negative stiffness region of the FL curve without an explicit FV model. (Fig. 3.1.C)
- The Huxley model produces higher forces during concentric contraction near the $l_{CE_{opt}}$, correlating with higher contraction velocities. (Fig. 3.3.C)
- The initial peak of the force produced by the Huxley model was a consequence of intrinsic muscle stiffness, rather than damping caused by intrinsic muscle viscosity. (Fig. 3.2)
- The duration of the stiffness peak in the Huxley model was consistent with the SRS duration found in experimental data. (Subsec. 3.1.3)
- When the stiffness of the muscle's starting position on the force-length (FL) curve became less positive, more excitation was required to be able to achieve stabilisation. (Fig. 3.5 and Fig. 3.6)
- Muscles simulated by the Huxley model require lower excitation levels to stabilise the musculoskeletal system. (Fig. 3.5 and Fig. 3.6. As a result, it appears that the intrinsic stiffness of the Huxley model acts as a type of self-stabilising mechanism, reducing the need for muscle activation to some extent.
- Only with the Huxley model was stability achieved for all the tested stiffness regions. This means that intrinsic muscle stiffness affects the muscle range at which musculoskeletal stabilisation is possible. (Fig. 3.5 and Fig. 3.6)
- The cost function of the task performed by the Huxley model was more robust to the changing feedback variables that dominantly were responsible for muscle activation patterns. The higher feedback robustness is speculated to be a consequence of the self-stabilisation behaviour stemming from the intrinsic muscle stiffness in the Huxley model affecting reaching tasks. (Fig. 3.8)

The discussion section will go over the implications of these findings in more detail.

5 Discussion

Hypothesis 1: Positive SRS in the negative flank

All three models displayed an increased force production as a result of a small local stretch in the negative stiffness flank of the force-length (FL) curve, even the Huxley model which did not include an explicit force-velocity (FV) model. Furthermore, the Hill_expanded model contractile element (CE) length l_{CE} is consistently higher at lengths away from the optimal length $l_{CE_{opt}}$, causing lower PE forces at the same length. Lastly, it was observed that while stretch forces are similar across the models, the Huxley model produces significantly higher forces during contraction near the $l_{CE_{opt}}$.

After fitting responses to local stretches of varying muscle velocities v_{mtc} in Experiment 1b, it was found that the initial peak of the force produced by the Huxley model was a consequence of intrinsic muscle stiffness, rather than damping caused by intrinsic muscle viscosity. This means that the force was produced here as a response to muscle stretch, rather than muscle velocity. The maximum stiffness in the response of the Huxley model was also 296.37% higher than that of the Hill_expanded model, in addition to the former occurring roughly 2.5 – 3 times earlier than the latter. Meaning, the Huxley model shows a faster force response as a result of length change compared to the Hill_expanded model. Furthermore, the duration of the stiffness peaks in the Huxley model was consistent with the short-range stiffness (SRS) duration found in experimental data[2][44], meaning that the observed force peaks in the Huxley model are indeed likely to be associated with SRS. It was also found that the Huxley damping during the SRS duration also peaked early, though quickly dropped to negative values before stabilising around $0 Ns/m$.

Lastly, in experiment 1c the Hill_expanded model depicted very high PE forces at high muscle lengths. This contrasts with the higher CE forces of the Huxley model, which are correlated with higher contraction velocities. Finally, it was found that the SRS of the Huxley model has a significant effect on the shape of the FL curves, especially at high velocities. The higher SRS at high velocities could be an indication of an input range where the force response of the muscle contains a higher degree of uncertainty. According to Ballesteros, Chairez and Poznyak [45], a controller designed using optimal feedback control theory (OFC) that solves the problem using the Optimality principle will increasingly rely on inaccurate approximation when faced with system uncertainties. Valero-Cuevas *et al.* [46] argue that, when applying OFC methods to musculoskeletal systems, the inherent uncertainties in the models likely lead to instability[16]. As a result, the higher uncertainty in force production as a result of SRS scaling with velocity suggests that higher stretch- and contractile velocities could be an upper bound for where successful prediction using OFC is possible.

HYPOTHESIS 2: INTRINSIC STABILISATION OF HUXLEY

Three main conclusions can be drawn from the results of experiment 2.

1. When the stiffness of the muscle's starting position on the force-length (FL) curve became less positive, more excitation was required in order to be able to achieve stabilisation, for all the models. The fact that a less positive FL stiffness means less muscle force is produced for an equal change of muscle length is in line with this result, as the muscles would need a higher excitation level to achieve the same force production for the same length and velocity changes.

2. In all cases, muscles simulated by the Huxley model require lower excitation levels to stabilise the musculoskeletal system through co-activation, in all stiffness regions and for both musculoskeletal systems. This suggests that the intrinsic stiffness of the Huxley model effectively acts as a self-stabilising mechanism, reducing the need for muscle activation to some extent. Implications for this range from reduced energy expenditure for this particular stabilisation strategy to a higher possible margin of stability being enabled by the intrinsic muscle stiffness.

3. Muscles simulated by the Huxley model were able to achieve stabilisation within the predefined terms in all cases. Even for the negative stiffness region simulations, where none of the Hill-type models were able to achieve successful stabilisation, the Huxley model was. As a result, it can be concluded that intrinsic muscle stiffness calculations play a significant role in the co-contraction stabilisation strategy for muscle length regions that would theoretically be considered unstable. Consequently, the muscle length range at which musculoskeletal stabilisation is possible appears to be larger for muscle models that include SRS behaviour. It also follows that intrinsic muscle stiffness might also affect stabilisation ranges for systems that include more types of inherent instabilities. Lastly, the fact that that these conclusions hold in both the 1DoF and the 2DoF cases could indicate that intrinsic muscle stiffness likewise influences the stabilisation of more complex musculoskeletal models.

HYPOTHESIS 3: HUXLEY IS MORE ROBUST

Robustness was assessed in three parts. First, a feedback system affecting muscles individually was designed. Next, optimal variables for the feedback system were found for a task where the optimal trajectory is already known. Finally, the individual feedback variable parameter space was explored. Precisely, the degree to which the cost changed was measured against how much individual parameters were scaled. This allowed for a comparison of the robustness of the feedback variables between the Huxley and the Hill_expanded models. It was found that the cost function of the task performed by the Huxley model was more robust to the changing feedback variables that dominantly were responsible for muscle activation patterns. However, the cost function of the task performed by the Hill_expanded model was more robust to the changing feedback variables that were insignificantly responsible for muscle activation patterns. It can then be concluded that the Huxley model allows for a higher degree of robustness in feedback variables. It is speculated that the higher feedback robustness in the Huxley model, which is essentially a form of self-stabilisation in reaching movements, is again a consequence of the intrinsic stiffness.

5.1. LIMITATIONS

5.1.1. GENERAL SHORTCOMINGS

The accuracy of the results of all experiments could have been improved by increasing the number of Hill-type and Huxley-type variations that are compared. This would have allowed for statistical analysis, where conclusions could have been drawn from many implementations of the models, which would mean the conclusions drawn can not simply have arisen from artefacts of individual models. Such a larger comparison could have led to an analysis of different control strategies that might have been affected by these other nonlinear muscle phenomena. More cross-bridges for the Huxley model could have improved accuracy, as well as drift correction for both of the integration methods. More reaching directions would have allowed for statistical analysis of the robustness of the feedback parameters, which likewise would have improved accuracy. The feedback system also has no basis in literature or biology, which could be improved. Furthermore, the magnitude of force and stiffness could not be compared with experimental SRS data, as an $f_{max} = 1$ is used, which is not biologically realistic.

5.1.2. PARAMETER RELIABILITY AND VALIDATION

The parameters used in this experiment are all directly taken from the literature. As no physical experiments have been performed, there was no set of data that any muscle model parameters could have justifiably been fit on. This means that the experiments leave a lot to be desired in terms of validation. The verification methods that worked were that the series element (SE) and the CE+PE force had to be equal in addition to the successful replication of previous simulations of other studies, though verification is not validation. This meant that certain sets of variables found in the literature were fitted to each other, and although these variables are based on experimental data, the type of muscle that those experimental datasets can vary dramatically from the type of muscle simulated in the experiments of this paper. As a consequence, the muscle parameters were often not (entirely) correct for the muscles that have been simulated. It should be noted that all the muscle models used the same set of parameters, meaning that the found results should still hold.

5.2. RECOMMENDATIONS

First of all, as the Vardy *et al.* [11] model may provide better estimates for muscle force and metabolic energy consumption when binding parameters are estimated from in vivo data, future research should repeat these experiments with such data. Moreover, as a result of findings in experiment 1c that link muscle velocity to uncertainty in force production, it appears that the prediction accuracy of OFC at higher muscle velocities could be an interesting area for future research. Based on the results from Experiment 2, which show that intrinsic muscle stiffness affects the degree to which muscles need to be excited to achieve successful stability through co-contraction, it follows that other neural

strategies that can be used to achieve stabilisation could likewise be affected. This seems like an interesting area for future research. In addition to that, because the range of muscle length where stability is possible is affected by intrinsic muscle stiffness, it appears interesting to research how intrinsic muscle stiffness affects stabilisation possibilities in other types of unstable musculoskeletal configurations. On top of that, as these conclusions hold for both the 1DoF and the 2DoF cases, future research should look into how intrinsic muscle stiffness influences the stabilisation of more complex musculoskeletal models.

The effect of intrinsic versus augmented stiffness could also be explored by comparing different muscle models, such as the Huxley-type model to a Hill-type model augmented with SRS, such as the one proposed by De Groote, Allen and Ting [3]. In addition to this, the effect of a larger amount of nonlinear muscle phenomena on control parameters could be investigated, such as force enhancement[10].

Finally, investigating the effects of intrinsic stiffness on the control parameters of a more sophisticated controller could provide a better comparison between neural and OFC controllers. Redoing experiment 3 with more reaching directions and a biologically plausible feedback system would also provide more definitive results.

BIBLIOGRAPHY

[1] P. M. Rack and D. Westbury. 'The short range stiffness of active mammalian muscle and its effect on mechanical properties'. In: *The Journal of physiology* 240.2 (1974), pp. 331–350.

[2] T. Franzen. 'Modelling Short-Range Stiffness: Comparison Between Hill-and Huxley-type Muscle Models'. In: (2019).

[3] F. De Groote, J. L. Allen and L. H. Ting. 'Contribution of muscle short-range stiffness to initial changes in joint kinetics and kinematics during perturbations to standing balance: A simulation study'. In: *Journal of biomechanics* 55 (2017), pp. 71–77.

[4] X. Hu, W. M. Murray and E. J. Perreault. 'Muscle short-range stiffness can be used to estimate the endpoint stiffness of the human arm'. In: *Journal of Neurophysiology* 105.4 (2011). PMID: 21289133, pp. 1633–1641. DOI: 10.1152/jn.00537.2010. eprint: https://doi.org/10.1152/jn.00537.2010. URL: https://doi.org/10.1152/jn.00537.2010.

[5] M. Shabani and I. Stavness. 'Simulating the effect of muscle stiffness and co-contraction on postural stability'. In: *Computer Methods in Biomechanics and Biomedical Engineering: Imaging & Visualization* 6.5 (2018), pp. 508–519.

[6] A. V. Hill. 'The heat of shortening and the dynamic constants of muscle'. In: *Proceedings of the Royal Society of London. Series B-Biological Sciences* 126.843 (1938), pp. 136–195.

[7] R. B. Stein, P. H. Peckham and D. P. Popovi. *Neural Prostheses, Replacing Motor Function After Disease Or Disabilities*. Oxford University Press, 1992. ISBN: 0-19-507216-2.

[8] A. F. Huxley. 'Muscle structure and theories of contraction'. In: *Prog. Biophys. Biophys. Chem* 7 (1957), pp. 255–318.

[9] H. Kim, T. G. Sandercock and C. J. Heckman. 'An action potential-driven model of soleus muscle activation dynamics for locomotor-like movements'. In: *Journal of Neural Engineering* 12.4 (June 2015), p. 046025. DOI: 10.1088/1741-2560/12/4/046025. URL: https://doi.org/10.1088/1741-2560/12/4/046025.

[10] J. Winters. 'Hill-Based Muscle Models: A Systems Engineering Perspective'. In: Jan. 1990, pp. 69–93. ISBN: 978-1-4613-9032-9. DOI: 10.1007/978-1-4613-9030-5_5.

[11] A. N. Vardy, K. K. Lemaire, A. J. Soest, F. C. van der Helm and E. de Vlugt. 'A generic state space Huxley muscle-tendon model'.

[12] S. Stroeve. 'Neuromuscular control model of the arm including feedback and feedforward components'. In: *Acta psychologica* 100.1-2 (1998), pp. 117–131.

[13] T. Flash and N. Hogan. 'The coordination of arm movements: an experimentally confirmed mathematical model'. In: *Journal of neuroscience* 5.7 (1985), pp. 1688–1703.

[14] D. McNamee and D. M. Wolpert. 'Internal models in biological control'. In: *Annual review of control, robotics, and autonomous systems* 2 (2019), pp. 339–364.

[15] E. Todorov and M. I. Jordan. 'Optimal feedback control as a theory of motor coordination'. In: *Nature neuroscience* 5.11 (2002), pp. 1226–1235.

[16] G. E. Loeb. 'Optimal isnt good enough'. In: *Biological cybernetics* 106 (2012), pp. 757–765.

[17] N. Mehrabi, R. Sharif Razavian, B. Ghannadi and J. McPhee. 'Predictive simulation of reaching moving targets using nonlinear model predictive control'. In: *Frontiers in computational neuroscience* 10 (2017), p. 143.

[18] E. de Vlugt, F. C. van der Helm, A. C. Schouten and G. G. Brouwn. 'Analysis of the reflexive feedback control loop during posture maintenance'. In: *Biological cybernetics* 84 (2001), pp. 133–141.

[19] E. de Vlugt. *Identification of spinal reflexes*. Citeseer, 2004.

[20] J. M. Winters and L. Stark. 'Muscle models: what is gained and what is lost by varying model complexity'. In: *Biological cybernetics* 55.6 (1987), pp. 403–420.

[21] T. L. Allinger, M. Epstein and W. Herzog. 'Stability of muscle fibers on the descending limb of the force-length relation. A theoretical consideration'. In: *Journal of biomechanics* 29.5 (1996), pp. 627–633.

[22] W. Herzog. 'The mysteries of eccentric muscle action'. In: *Journal of sport and health science* 7.3 (2018), p. 253.

[23] D. Knudson. 'The biomechanics of stretching'. In: *Journal of Exercise Science and Physiotherapy* 2 (2006), pp. 3–12.

[24] A. V. Hill. 'The Series Elastic Component of Muscle'. In: *Proceedings of the Royal Society of London. Series B, Biological Sciences* 137.887 (1950), pp. 273–280. ISSN: 00804649. URL: http://www.jstor.org/stable/82551.

[25] G. Shue, P. Crago and H. Chizeck. 'Muscle-joint models incorporating activation dynamics, moment-angle, and moment-velocity properties.' In: *Biomedical Pharmacology Journal* 42 2 (1995), pp. 212–23. DOI: 10.1109/10.341834.

[26] R. D. Astumian. 'Huxley's Model for Muscle Contraction Revisited: The Importance of Microscopic Reversibility'. In: *Polymer Mechanochemistry*. Ed. by R. Boulatov. Cham: Springer International Publishing, 2015, pp. 285–316. ISBN: 978-3-319-22825-9. DOI: 10.1007/128_2015_644. URL: https://doi.org/10.1007/128_2015_644.

[27] C. Y. Seow. 'Hills equation of muscle performance and its hidden insight on molecular mechanisms'. In: *Journal of General Physiology* 142.6 (2013), pp. 561–573.

[28] M. M. Panjabi *et al.* 'The stabilizing system of the spine. Part II. Neutral zone and instability hypothesis'. In: *Journal of spinal disorders* 5 (1992), pp. 390–390.

[29] B. A. Knarr, J. A. Zeni Jr and J. S. Higginson. 'Comparison of electromyography and joint moment as indicators of co-contraction'. In: *Journal of Electromyography and Kinesiology* 22.4 (2012), pp. 607–611.

[30] J. He, M. Maltenfort, Q. Wang and T. Hamm. 'Learning from biological systems: modeling neural control'. In: *IEEE Control Systems Magazine* 21.4 (2001), pp. 55–69. DOI: 10.1109/37.939944.

[31] V. C. Cheung, B. M. Cheung, J. H. Zhang, Z. Chan, S. C. Ha, C.-Y. Chen and R. T. Cheung. 'Plasticity of muscle synergies through fractionation and merging during development and training of human runners'. In: *Nature communications* 11.1 (2020), pp. 1–15.

[32] S. Dehghani and F. Bahrami. 'How does the CNS control arm reaching movements? Introducing a hierarchical nonlinear predictive control organization based on the idea of muscle synergies'. In: *PloS one* 15.2 (2020), e0228726.

[33] M. L. Latach. *Synergy*. Oxford University Press, 2008. ISBN: 978-0-19-533316-19.

[34] E. N. Marieb and K. Hoehn. *Human Anatomy & Physiology*. 11. Pearson, 2019. ISBN: 978-1-292-26103-4.

[35] F. E. Zajac. 'Muscle and tendon: properties, models, scaling, and application to biomechanics and motor control.' In: *Critical reviews in biomedical engineering* 17.4 (1989), pp. 359–411.

[36] F. Romero and F. J. Alonso. 'A comparison among different Hill-type contraction dynamics formulations for muscle force estimation'. In: *Mechanical Sciences* 7.1 (2016), pp. 19–29. DOI: 10.5194/ms-7-19-2016. URL: https://ms.copernicus.org/articles/7/19/2016/.

[37] L. Vannucci, E. Falotico and C. Laschi. 'Proprioceptive Feedback through a Neuromorphic Muscle Spindle Model'. In: *Frontiers in Neuroscience* 11 (2017). ISSN: 1662-453X. DOI: 10.3389/fnins.2017.00341. URL: https://www.frontiersin.org/article/10.3389/fnins.2017.00341.

[38] R. H. Miller. 'Hill-Based Muscle Modeling'. In: *Handbook of Human Motion*. Ed. by B. Müller, S. I. Wolf, G.-P. Brueggemann, Z. Deng, A. McIntosh, F. Miller and W. S. Selbie. Cham: Springer International Publishing, 2018, pp. 1–22. ISBN: 978-3-319-30808-1. DOI: 10.1007/978-3-319-30808-1_203-2. URL: https://doi.org/10.1007/978-3-319-30808-1_203-2.

[39] G. I. Zahalak. 'A distribution-moment approximation for kinetic theories of muscular contraction'. In: *Mathematical biosciences* 55.1-2 (1981), pp. 89–114.

[40] J. Wu, W. Herzog and G. Cole. 'Modeling dynamic contraction of muscle using the cross-bridge theory'. In: *Mathematical biosciences* 139.1 (1997), pp. 69–78.

[41] D. G. Thelen. 'Adjustment of muscle mechanics model parameters to simulate dynamic contractions in older adults'. In: *J. Biomech. Eng.* 125.1 (2003), pp. 70–77.

[42] C. C. Raasch and F. E. Zajac. 'Locomotor strategy for pedaling: muscle groups and biomechanical functions'. In: *Journal of neurophysiology* 82.2 (1999), pp. 515–525.

[43] R. Shadmehr and F. A. Mussa-Ivaldi. 'Adaptive representation of dynamics during learning of a motor task'. In: *Journal of neuroscience* 14.5 (1994), pp. 3208–3224.

[44] S. Van Eesbeek, J. H. De Groot, F. C. Van der Helm and E. De Vlugt. 'In vivo estimation of the short-range stiffness of cross-bridges from joint rotation'. In: *Journal of biomechanics* 43.13 (2010), pp. 2539–2547.

[45] M. Ballesteros, I. Chairez and A. Poznyak. 'Robust optimal feedback control design for uncertain systems based on artificial neural network approximation of the Bellmans value function'. In: *Neurocomputing* 413 (2020), pp. 134–144.

[46] F. J. Valero-Cuevas, H. Hoffmann, M. U. Kurse, J. J. Kutch and E. A. Theodorou. 'Computational models for neuromuscular function'. In: *IEEE reviews in biomedical engineering* 2 (2009), pp. 110–135.

[47] H. Vallery and A. L. Schwab. *Advanced Dynamics*. Delft University of Technology, 2020.

A PARAMETERS

A.1. EXPERIMENT PARAMETERS

This section contains a list of all the parameters used in this thesis.

Symbol	Value	Unit	Description	Source
Environment	parameters		-	-
l_1	0.32	[m]	Length of upper arm	[12]
l_2	0.32	[m]	Length of lower arm	[12]
l_3	0.125	[m]	Shoulder muscle attachment	[12]
l_4	0.125	[m]	Elbow muscle attachment	[12]
m_1	1.8	[kg]	Mass of upper arm	[12]
m_2	0.4	[kg]	Mass of lower arm	[12]
m_3	1.0	[kg]	Mass of lower arm	
J_1	0.015	$[kg \cdot m^2]$	Inertia of upper arm	[12]
J_2	0.013	$[kg \cdot m^2]$	Inertia of lower arm	[12]
J_3	0.0008	$[kg \cdot m^2]$	Inertia of ball (circle)	
r_1	0.05	[rad]	Shoulder radius	[12]
r_2	0.05	[rad]	Elbow radius	[12]
B_1	0.3	$[Nm \cdot s/rad]$	Shoulder damping	[12]
B_2	0.2	$[Nm \cdot s/rad]$	Elbow damping	[12]
θ_{r1}	$\pi/3$	[rad]	Shoulder rest angle	[12]
θ_{r2}	$\pi/2$	[rad]	Elbow rest angle	[12]
PE_{sh1}	18	[-]	Shoulder PE shape (for damping calc.)	[12]
PE_{sh2}	18	[-]	Elbow PE shape (for damping calc.)	[12]
PE_{xm1}	$\pi/2$	[rad]	Shoulder PE range (for damping calc.)	[12]
PE_{xm2}	$\pi/2$	[rad]	Elbow PE range (for damping calc.)	[12]
Huxley	parameters		-	-
f	275.8722	[-]	Constant used in the f function	[11]
g1	176.6001	[-]	Constant used in the g function	[11]
g2	1065.6713	[-]	Constant used in the g function	[11]
g3	305.0962	[-]	Constant used in the g function	[11]
h_{mtc}	2.8418E-008	[m]	maximum cross-bridge length	[11]
s_{mtc}	2.6E-6	[m]	cross-bridge length	[11]
t_{act}	40	[ms]	activation constant	[42]
t_{deact}	70	[ms]	deactivation constant	[42]
$l_{se_{slack}}$	$0.2 \cdot l_{CE_{opt}}$	[m]	SE slack length	
$l_{pe_{slack}}$	$1.3 \cdot l_{CE_{opt}}$	[m]	PE slack length	[11]
PE_{sh}	3	[-]	PE shape factor (for stiffness calc.)	[11][41]
SE_{sh}	5	[-]	SE shape factor (for stiffness calc.)	[11][41]
PE_{xm}	0.06	[-]	isometric passive strain factor (for stiffness calc.)	[11][41]
SE_{xm}	0.6	[-]	isometric tendon strain factor (for stiffness calc.)	[11][41]
SE_{ftoe}	0.33	[-]	Toe region exponential shape factor	[11][41]

Table A.1.: List of all non Hill-specific parameters used, based on Experiment 2b, Fig. 2.4.B. For Experiment 2a, m_2 and J_2 values were set to the m_3 and J_3 values of this table. In Experiment 2a and 2c, m_3 and J_3 values did not apply. For Experiment 1, environment parameters did not apply.

Parameter	m_1	m_2	m_3	m_4	m_5	m_6	Unit
θ_{act}	40	40	40	40	40	40	ms
θ_{act}	70	70	70	70	70	70	ms
r_{i1}	0.03	0.03	0	0	0.025	0.025	m
r_{i2}	0	0	0.03	0.03	0.04	0.04	m
F_{max}	2000	2000	900	900	600	600	N
l_r	0.15	0.15	0.15	0.15	0.35	0.35	m
l_t	0.02	0.02	0.02	0.02	0.04	0.04	m
L_{opt}	0.7	0.7	0.7	0.7	0.7	0.7	-
L_{sh}	0.6	0.6	0.6	0.6	0.6	0.6	m
V_{er}	0.5	0.5	0.5	0.5	0.5	0.5	-
V_{ml}	1.3	1.3	1.3	1.3	1.3	1.3	-
V_{vm}	$6{\cdot}lce_0$	$6{\cdot}lce_0$	$6{\cdot}lce_0$	$6{\cdot}lce_0$	$6{\cdot}lce_0$	$6{\cdot}lce_0$	m/s
V_{sh}	0.3	0.3	0.3	0.3	0.3	0.3	-
V_{shl}	0.23	0.23	0.23	0.23	0.23	0.23	-

Table A.2.: List of all Hill-specific muscle parameters used, directly copied from Stroeve [12].

A.2. STIFFNESS REGIONS

		long muscle			short muscle		
stiffness region	region number	$l_{CE_{opt}}$	l_{CE_0}	δ_l	$l_{CE_{opt}}$	l_{CE_0}	δ_l
High positive	1	0.29284	0.25798	0.03492	0.13524	0.09133	0.04391
Medium positive	2	0.28000	0.26064	0.01936	0.12240	0.09405	0.02835
Low positive	3	0.26716	0.26336	0.00390	0.10956	0.09677	0.01279
Low negative	4	0.25432	0.26608	-0.01176	0.09672	0.09950	-0.0028
High negative	5	0.24148	0.26881	-0.02733	0.08388	0.10222	-0.01834

Table A.3.: Table containing information regarding the values for the stiffness regions

B EXTENDED METHODS

B.1. ENVIRONMENT SYSTEM CALCULATION: TMT METHOD

In this subsection the mathematical derivation behind the system physics is shortly explained[47]. In the following vector notations the referred dimensionality is seen in Eq. B.1 and Eq. B.2.

$$i,k = 1..n \tag{B.1}$$

$$j,l,m = 1..d \tag{B.2}$$

Here d is the number of generalised coordinates and n is the number of rigid bodies. This method starts with the virtual power of applied forces with d'Alambert's inertial forces $-M_{ik}\ddot{x_k}$ and generalised forces Q_j in Eq. B.3.

$$\delta P = \delta\dot{i}(F_i - M_{ik}\ddot{x_k}) + \delta\dot{q_j}Q_j \tag{B.3}$$

The kinematic constraints in which system is in equilibrium are given in Eq. B.4.

$$C_{k,i}\delta\dot{x_i} = 0 \tag{B.4}$$

Then the virtual velocities which satisfy the constraints are given in Eq. B.5.

$$\delta\dot{x_i} = T_{i,j}\cdot\delta q_j \tag{B.5}$$

The accelerations which satisfy the constraints are in Eq. B.6.

$$\ddot{x_k} = T_{k,l}\ddot{q_l} + T_{k,lm}\dot{q_l}\dot{q_m} \tag{B.6}$$

The system is in dynamic equilibrium when Eq. B.7 is true.

$$\delta P = 0 \forall \delta\dot{q_j} \tag{B.7}$$

This results in the following equations of motion in Eq. B.8.

$$T_{i,j}M_{ik}T_{k,l}\ddot{q_l} = Q_j + T_{i,j}(F_i - M_{ik}g_k) \tag{B.8}$$

Where g_k are the convective acceleration terms in Eq. B.9.

$$g_k = T_{k,lm}\dot{q_l}\dot{q_m} \tag{B.9}$$

$T_{k,l}$ is the Jacobian matrix where Eq. B.10 holds

$$T^T_{k,l} = T_{i,j} \tag{B.10}$$

It is found through the virtual velocity equation [47]. M_{ij} refers to the mass matrix for bodies in Newtonian reference frame system[47]. q_j is the generalised coordinate vector. F_i is the force and torque vector $F_i = (J_i, F_x, F_y)_b)$. In all experiments, the system state variables describing the environment calculated using the TMT method were updated every time step using an rk4 integrator.